Understanding Therapeutic Monoclonal Antibody Aggregation Mechanisms through Biophysical, Biochemical and Biological Characterization of Two Types of Immunoglobulin G Dimers

By
Christopher E. Woods

Submitted to the graduate degree program in Pharmaceutical Chemistry and the Graduate Faculty of the University of Kansas in partial fulfillment of the requirements for the degree of Master of Arts.

_____
Chairperson, Professor David Volkin

_____
Dr. Feng He, Amgen Representative

_____
Professor Thomas Tolbert

Date Defended: June 26, 2015

The Thesis Committee for Christopher E. Woods

Certifies that this is the approved version of the following thesis:

Understanding Therapeutic Monoclonal Antibody Aggregation Mechanisms through Biophysical, Biochemical and Biological Characterization of Two Types of Immunoglobulin G Dimers

_____

Chairperson, Professor David Volkin

Date Approved: July 1, 2015

ABSTRACT

Aggregation has been identified as one of the major degradation pathways that affect the quality and efficacy of protein therapeutics. Dimers are one of the predominant oligomeric species found in monoclonal antibody (mAb) based products, whose formation can occur both during processing and long-term storage, and following exposure to certain accelerated stress conditions. It has been hypothesized that these dimeric species could be the initial step on the mAb protein aggregation pathway, but this has been difficult to establish since mAb dimers can be a heterogeneous population of molecules. In this study, two mAb dimer species were generated and isolated from IgG2 monoclonal antibody samples, one upon long-term storage and the other from elevated stress conditions. The dimer-enriched fractions were characterized for protein conformation, morphology, structural integrity and bioactivity. The results revealed both common properties and unique differences between the two types of mAb dimers generated under these two different conditions. The findings of this study provide insights towards greater understanding of the possible causes of dimer formation under native storage and thermal stress conditions for this IgG2 mAb, and two possible mechanisms of dimer formation are proposed.

ACKNOWLEDGEMENTS

I must begin all acknowledgments with my MS thesis advisors, Dr. Feng He and Professor David Volkin. I offer them my immense gratitude for their vital roles in guiding the research described in this thesis, providing helpful feedback, suggestions for improvement, encouragement, patience and support.

My sincere appreciation goes to all of my collaborators from Amgen for generously offering their knowledge, expertise and time to provide data critical to understanding the problems addressed in this thesis: Joey Pollastrini, Dr. Vladimir Razinkov, Dr. Feng He and Mei Han for their contributions to the SEC-MALS, SV-AUC, CD and FTIR spectroscopy and SDS-PAGE data and analysis, respectively. Dr. Peter Zhou, Edith Nalbandian and Gwen Maher for their contributions to the AFM image analysis, Potency, and FcRn binding data, respectively.

I would especially like to thank Dr. Jun Zhang for the extraordinary amount of time and expertise he contributed by performing H/D-MS analysis, limited proteolysis and disulfide peptide mapping data. The contributions he has made to this work have been inspiring and invaluable. Some of these results, as related to mAb dimer formation, are summarized in this thesis, and much of this work will be presented in a separate manuscript (in preparation).

I would like to thank all of the Amgen scientific leaders who have provided meaningful discussions, insightful feedback and continued support for this project during our time at Amgen together: Drs. Gerald Becker, Bruce Kerwin, Linda Narhi and Michael Treuheit.

I close the acknowledgements by thanking Professor Thomas Tolbert at the University of Kansas for agreeing to be a committee member for the review of this work.

TABLE OF CONTENTS

INTRODUCTION

Importance of Understanding Monoclonal Antibody Aggregation

Monoclonal antibodies (mAbs), specifically those of the immunoglobulin G (IgG) subclass, have become important therapeutic options for a variety of diseases. As of 2014, more than ~50 mAb drug products have been approved by regulatory agencies in the US and Europe[1]. Compared to small molecule drugs, the structural complexity of IgG mAb-based drug products are orders of magnitude greater, due not only to their much higher molecular weight but also as a consequence of post-translational modifications and their folded, delicate three dimensional structure. This results in significant challenges for biopharmaceutical manufacturers attempting to ensure the safety, efficacy and quality of their products during manufacturing, storage and administration.

Antibodies, which play a critical role in the functioning of the immune system, are produced in vivo by plasma cells and are classified by isotypes that differ in structure and function. Five major antibody isotypes have been identified in mammals: IgA, IgD, IgE, IgG and IgM. This work focuses on an IgG mAbs produced at large scale by cell culture. An IgG mAb is a large glycoprotein molecule formed by covalent and non-covalent interactions of four polypeptide chains. A schematic representation of an IgG2 mAb is shown in Figure 1. Each of two identical light chains (~25 kDa each) are attached to each of two identical heavy chains (~50 kDa) by an inter-chain disulfide bond. The light chain contains two Ig domains (V_L, C_L) while the heavy chain has four Ig domains (V_H, C_H1, C_H2, C_H3). The two heavy chains are joined together by four inter-chain disulfide bonds, at a region known as the hinge, resulting in a

quaternary structure with two identical halves. The resulting homodimeric monomer has a molecular weight (MW) of approximately 150 kDa.

A mAb molecule is commonly described by two biologically functional regions: the fragment antigen binding (Fab) domain and the fragment crystallizable (Fc) domain. The Fab domain, located above the hinge, consists of each of the two arms that form the characteristic "Y" shape of the IgG molecule. At the N-terminus of each Fab, the variable domains of the heavy (V_H) and light (V_L) pair together to form the binding sites (CDRs) specific to the targeted epitope of the antigen (See Figure 1). The Fc domain, located below the hinge, consists of the two heavy chain constant domains, C_H2 and C_H3, which interact pair-wise across the two identical heavy chains via non-covalent interactions. The Fc domain contains a carbohydrate chain attached to an N-glycosylation site in the C_H2 domain. The carbohydrate chain is a post-translational modification that has been shown to be important for mediating effector function activities in vivo [2].

Of all the potential physicochemical degradation mechanisms associated with mAb therapeutics, controlling physical degradation due to aggregation is one of the biggest challenges facing biopharmaceutical development scientists [3-8]. Protein aggregates are commonly understood to encompass any assembly of protein species having higher molecular weight than the desired "native" species, in the case of an IgG mAb a single homodimeric monomer unit. Excessive protein aggregation has been viewed as a major threat to the quality of protein therapeutics, leading to the impurity of the active product and potential loss of efficacy and/or increase in immunogenicity upon administration [7, 9]. Throughout the manufacturing of protein therapeutics, environmental conditions pose significant stresses on the protein entity and may cause the protein to aggregate to non-native higher order structural forms [7, 10, 11]. Common

stress conditions include higher temperature, pH extremes, physical agitation, oxidation, etc. As advanced as cell culture and purification technologies have become at a manufacturing scale, it remains nearly impossible to completely exclude all the protein aggregates during the expression and purification of the protein product. Furthermore, long term storage and distribution process of the protein therapeutic dosage forms may cause additional aggregation to occur prior to or potentially even during administration to patients.

Understanding the Causes of mAb Aggregation

The molecular mechanisms that initiate and propagate mAb aggregation have been shown to be variable in nature: pre-existing chemical degradation of the protein (e.g., oxidation), partial unfolding, unpaired free cysteine residues, and overly exposed hydrophobic regions on the polypeptides. In addition, colloidal stability is also very important in terms of the propensity to have random collisions between protein molecules [8, 12-16]. It is reasonable to assume that the precise mechanism of mAb aggregation highly depends on environmental stress, the formulation solution conditions and the vulnerability of the individual mAb molecule itself to undergo structural alterations preceding the aggregation event, i.e., chemical change, physical change or other degradations that already exist in the monomeric form. Developing a better understanding and deciphering the protein aggregation mechanisms will help to minimize its occurrence by circumventing conditions that are likely to trigger such events or avoiding mAb entities that have a greater tendency to aggregate.

Many literature reports have hypothesized that reversible and irreversible dimerization formation, occurring via the joining of two mAb monomers through covalent or non-covalent interactions, serves as the initial step of protein aggregation. As shown in Figure 2, adapted from

Roberts, et al [17], protein aggregates are thought to form through a variety of steps, usually first involving a partial unfolding of the native protein structure. A partially unfolded monomer may interact with the native monomers, or other partially unfolded monomers in solution, to form reversible self-associated oligomers. Associations of two, three or four monomer units are referred to as a dimer, trimer, tetramer, respectively. At some point, structural or conformational changes to the self-associated oligomers may occur, leading to intermolecular interactions that are non-reversible. At this stage, the protein oligomers exist as a soluble aggregate containing a number of monomer units. The formation of an irreversible dimer species of an IgG2 mAb is the focus of this work. As shown in Figure 2, monomers, with either native or partially unfolded structure, may continue adding to the soluble aggregate to grow the aggregate structure into a high molecular weight (HMW) species. Likewise, soluble aggregates may interact with each other in solution to form even larger HMW species. When growth of aggregate species causes a change in the solubility of the protein, it may precipitate out of solution via phase separation leading to the formation protein particles of varying size and physical characteristics (e.g., submicron, sub-visible and visible particles)[18].

Not all multimeric species of immunoglobulin are necessarily detrimental, especially forms produced in vivo as part of the immune system. Indeed, IgA and IgM antibody isotypes are known to form naturally occurring oligomers that have important roles as a first line of immune defense secretory immune system [19]. The biosynthesis of the IgA and IgM monomers typically occur in secretory epithelial cells through the involvement of a small joining peptide, known as the J-chain. The J-chain forms disulfide bonds with cysteine residues near the C-terminal ends of the Fc domains of two IgA monomers. In the case of IgM, one J-chain is responsible for forming a dimer of two IgM monomers, and the remaining monomers that form

the IgM pentamer are linked together through additional disulfide bonding at the tail end of the Fc domains. In both cases, IgA and IgM molecules are joined at the tail ends of the Ig monomers, resulting in the outward orientation of the antigen-binding domains. One of the main features of polymeric IgA and IgM antibodies is the increased valency of the antigen-binding domains. The close proximity of multiple antigen-binding sites improves the probability of epitope binding. Additionally, multiple bacterial or viral cells may be clumped together by the same polymeric antibody, thus preventing permeation of the pathogens through mucosal membranes. Because secretory IgA and IgM oligomers are joined through the Fc regions, they show little to no activation of the complement immune system, which allows the clearance of pathogens from mucosal membrane surfaces without inducing an inflammatory response. The features of naturally occurring IgA and IgM oligomers may, in theory, have practical implications for therapeutic IgG oligomers. For example, an improved therapeutic potency could be observed in IgG mAb oligomers if the additional valency of the Fab domains results in a greater probability for antigen binding relative to the IgG mAb monomer.

Since in the case of IgG mAbs, dimer populations have been shown to be quite heterogeneous in nature, it is unclear whether some types of IgG dimers are more prone to growing into larger oligomers than others [4, 20-23]. Several studies have implicated non-covalent interactions between the Fab domains as a root cause of dimer formation [21, 24-27]. Others have shown that covalent interactions caused by disulfide bond rearrangements are to blame for dimer formation [12, 16, 23, 28]. Van Buren et al found that, depending on the pH of the mAb solution, distinct dimer formation pathways could be detected [23]. Recently, Paul et al showed detailed characterization of mAb dimers induced by purification stress, low pH and photo exposure [29]. The study demonstrated, although similar in size, mAb dimers exhibit

drastically different physical and chemical properties, which may also impact biological functions.

Recently, investigations of IgG dimers by Hydrogen/Deuterium Exchange Mass Spectrometry (H/D-MS) has emerged as a very sensitive, high-resolution approach to understanding the interaction sites between two monomers at the dimer interface. For example, Iacob, et al have investigated the properties of IgG dimers formed after manufacturing from IgG1 and IgG2 solutions [30], and were able to identify the role of C_H2 domain disulfide bonds as the cause of dimer formation in an IgG2 mAb. Interestingly, Zhang, et al, were able to identify regions in the Fab domain of an IgG1 mAb that were susceptible to protein aggregation upon thermal and freeze-thaw stress [31].

The Problem—The Causes of IgG Dimer Formation in Monoclonal Antibody Formulations Remain Ambiguous

Although many analytical methods are routinely employed for the detection and quantification of protein aggregates, such methods are often limited in their ability to characterize the detailed structural differences that lead to their formation and to subsequent larger protein aggregates. Various pathways for mAb aggregation have been proposed in the literature, but knowledge about the mechanisms that control of mAb aggregation remains limited. Furthermore, the structural aspects of dimer formation, the smallest form of protein aggregate, and their role in the overall protein aggregation pathway, are not well understood. It is hoped that upon identifying the detailed properties of the aggregated mAb dimer formed by different stresses, the causes and mechanisms of protein aggregation can be better characterized and controlled during the formulation development cycles (from lab to clinical trials to commercial manufacturing).

The Hypothesis

Formulation scientists are responsible for developing pharmaceutical dosage forms that preserve the physiochemical properties of therapeutic mAb solutions for an extended period of time, usually greater than two years, in order to satisfy the demand for clinical trial material, and upon approval, to offer favorable supply-chain conditions. Successful protein therapeutic formulations are highly robust under a variety of handling conditions, show lower relative rates of protein degradations and provide the longest possible expiry for the drug product. Typically, mAb formulations are compared for their relative rates of degradation under a variety of storage temperatures as a function of time. One of the primary degradation mechanisms observed during formulation development is protein aggregation, with mAb dimer being the primary type of mAb aggregate found under both low temperature storage and accelerated stability evaluations at higher temperatures. Since the role dimer plays in the overall protein aggregation pathway of monoclonal antibodies is not well understood, the focus of this investigation is to isolate two types of dimers from a specific IgG2 mAb: one formed during long-term storage at low temperature and the other formed during short exposure to high temperature stress. Because low and high temperatures are commonly evaluated during formulation development for protein therapeutic physiochemical stability, it is hoped that any observed similarities or differences between the isolated dimers will lead to better understanding of the potential mechanisms of mAb dimer/ aggregate formation under such conditions.

Upon successful isolation of dimeric mAb species, a number of physical, chemical and biological methods can be employed to understand the similarities and differences of the IgG2 mAb dimer types and how they compare to the native mAb monomer. A through analytical

characterization of the IgG2 dimer fractions may help to elucidate potential mechanisms of dimer formation for this IgG2 mAb under these two conditions. The results presented here will provide insights into the role of protein conformational changes may play during the aggregation of this IgG2 mAb monomer into dimers.

Analytical Techniques Utilized to Monitor Protein Aggregation

During biotherapeutic formulation development, protein product candidates are subjected to numerous stress conditions in order to accelerate the onset of protein aggregation. The results of these stress studies are often used to (1) identify stabilizing excipients and formulations, (2) confirm stability indication of analytical methods, and (3) to help predict the overall aggregation of a product prior to reaching the expiry. While the stress conditions vary, the detection and characterization of protein aggregates is mainly achieved by employing a standard set of qualitative and quantitative methods. For example, der Engelsman, et al have provided a comprehensive overview of the common analytical methods used to analyze protein aggregates along with their respective advantages and disadvantages[32]. In this study, a variety of analytical techniques are employed to assess protein size, structure, biological activity and chemical modifications of the dimer species of a model IgG2 mAb.

Size exclusion chromatography (SEC) is the workhorse for quantification of soluble protein aggregates. SEC, which measures the hydrodynamic radius of solute molecules, separates monomer from aggregate species by gel filtration. Assuming protein monomer and soluble aggregates have the same extinction coefficient, it is possible to quantify the extent of aggregation for a given sample by measuring UV absorption of the eluting protein species. Calibrating a column used in SEC with a reference solution containing protein molecules of

known molecular weight (MW) can be used to give an estimate of the mass of an unknown protein based upon elution position. Combining a SEC method with specialized light scattering equipment, a method known as size exclusion chromatography coupled with on-line multi angle light scattering (SEC-MALS), can provide accurate MW measurements for the monomeric and aggregated species in a protein solution. Sedimentation Velocity Analytical Ultracentrifugation (SV-AUC) is a size distribution technique that has been shown to be useful as an complimentary technique to SEC for detecting aggregated proteins[33]. SV-AUC has several advantages over SEC, including the ability to detect a larger size range of protein aggregates and reduces the potential for aggregate disruption by limiting buffer composition differences and surface interactions. SV-AUC has also been shown to distinguish different orientations of dimer species [29, 34]. In addition to separating proteins based on size distribution under native-like conditions, sodium dodecyl sulfate polyacrylamide gel electrophoresis (SDS-PAGE) can provide information on the MW size of the denatured forms of the proteins including the nature of bonding between protein oligomers [35].

Biophysical techniques such as Circular dichroism (CD) spectroscopy, Fourier transform infrared (FT-IR) spectroscopy and extrinsic fluorescence spectroscopy are commonly used for probing the higher-order structural integrity of mAbs. CD, which measures the difference in absorption of left-handed and right-handed circularly polarized light, has been widely used to study a protein's overall secondary and tertiary structure as an indicator of protein stability in solution [14, 36-41]. In the far-UV wavelength region, typically measured from 190-240 nm, amide bonds that form the peptide backbone are monitored as chromophores and the resulting CD absorption spectra are reflective of various secondary structural elements in proteins, such as α-helices, ß-sheets, ß-turns and unordered (or random coil) conformations. CD spectra obtained

in the near-UV wavelength region (250-350 nm) are the result of aromatic amino acids (i.e., tryptophan, phenylalanine and tyrosine) and disulfide bonds acting as chromophores. Because the features of a near-UV CD signal, such as intensity and sign (positive or negative), are dependent on the three-dimensional (3D) orientation of the chromophores within the protein structure, near-UV CD spectra provide tertiary structural information. Unlike far-UV CD, features of near-UV CD spectra cannot be assigned to a specific 3D structure. Rather, near-UV CD provides a spectral fingerprint for the native, folded protein that can be used to observe the impacts of any variety of alterations to the protein structure or its environment. For example, Li et al demonstrated the use of near-UV CD in manufacturability assessment screening by comparing the relative changes in tertiary structure of protein candidates induced by exposure to low pH [42].

FTIR spectroscopy is a type of absorption spectroscopy that is commonly applied for the investigation of a protein molecule's overall secondary structure content in solution as well as in the solid state. FTIR spectra result from passing a range of infrared light through a sample and measuring the amount of light absorbed at each frequency. The infrared light is absorbed when its frequency is equivalent to the vibrational frequency of a particular bond. FTIR is especially useful for observing the vibrational states associated of the protein backbone, particularly the amide I bond, which has been shown to exhibit characteristic absorption spectral features for different secondary structures, such as α-helices, ß-sheets and ß-turns [43]. FTIR has been shown to be useful for observing changes in a protein molecule's secondary structure content caused by chemical, thermal and mechanical stresses in both the liquid and solid states [4, 16, 38, 44-48].

Extrinsic fluorescence spectroscopy is a highly sensitive technique with many applications for use in the formulation development of biopharmaceutical drug products [49]. Extrinsic fluorescence spectroscopy measures the interaction of fluorescent probes with the protein of interest. Such probes, often small molecule dyes, can form covalent or non-covalent associations with the protein structure to reveal, depending on the dye, different properties of protein structure[50]. SYPRO® Orange has been demonstrated as a useful dye for monitoring protein unfolding and protein stability under thermal stress, as well as its ability to detect IgG aggregates during therapeutic protein development[51, 52]. In aqueous solutions, the fluorescent emission of SYPRO® Orange is insignificant. When the dye is able to bind or interact with hydrophobic amino acid residues or hydrophobic regions in a protein, a significant increase in fluorescent emission can be detected. It is generally accepted that, for a protein in its native state, thermodynamics of protein folding favor the hydrophobic amino acid residues be oriented toward the interior of the tertiary protein structure and away from the surface exposed to aqueous solvents (i.e., hydrophobic collapse). Therefore, fluorescent emission spectra increases of SYPRO® Orange dye upon heat exposure can be interpreted as a measure of protein unfolding.

Differential scanning calorimetry (DSC) is a tool used for measuring the thermal melting behavior of proteins, and many applications have been demonstrated that are specific to the development of biopharmaceutical drugs and their formulations [53]. DSC measures the difference in heat required to maintain synchronous temperature between a protein sample solution and a reference solution (containing only the formulation buffer) as the temperature is raised across the range being studied. The amount of energy necessary for maintaining constant temperature between the protein sample and reference is the heat capacity (C_p). Typically, molar C_p is plotted as a function of temperature (T), which provides the enthalpy (ΔH) of unfolding

caused by heat denaturation (assuming the unfolding event is reversible in nature). For either reversible or irreversible thermal transitions, the transition midpoint(s), (T_m) of thermal unfolding events, can be monitored. For protein molecules, T_m represents the temperature at which 50% of the protein retains its native conformation and 50% of the protein is heat-denatured. DSC analysis of mAbs have been shown the IgG molecules to exhibit multiple T_m values and can be attributed to the unfolding of specific domains, such as the C_H2 or Fab domains [54]. Generally, higher T_m values can be indicative of improved conformational stability, and consequently, DSC has been established as a vital tool in biopharmaceutical development. Examples of DSC applications include assessing the impacts of primary sequence mutations, protein candidate screening in early development, and formulation excipient screening, to name a few examples [55-58].

Most of the biophysical assays used to characterize protein aggregation are limited in their ability to identify the mechanism or pathways of protein aggregation because they generally provide global information averaged across the entire molecule, and are not sensitive enough to observe small changes in the molecular structures of proteins. Hydrogen–Deuterium Exchange Mass Spectrometry (H/D-MS) has emerged as a fast, high-resolution tool for detecting minor conformational changes in the structural dynamics of proteins at the molecular level [24, 30, 59-63]. H/D-MS has been proven capable of detecting chances in structural dynamics of mAbs that result from changes in formulation excipients[64, 65], characterizing protein aggregates[30, 66], impacts of chemical modifications on protein structure[31] and the effects of charge mutations on protein conformation[67], to name a few examples from the recent scientific literature.

The fundamental principle underlying H/D-MS analysis is ability to observe differences in the rates of deuterium exchange with amide hydrogen of the polypeptide backbone. For

example, hydrogen atoms in a random coil peptide (without higher-order structure), which is highly exposed to the solvent, will exchange with deuterium almost instantaneously (depending on solution pH and the inherent chemical exchange rate), whereas the hydrogen bonds of the amide backbone in a folded protein under the same conditions will exchange with deuterium at rates heavily influenced by the folded structure of the protein (as well as the inherent chemical exchange rate)[68]. When a protein structure is altered in such a way that it results in a conformational change with altered local flexibility, deuterium may exchange with the hydrogen of polypeptide backbone in a particular peptide segment at a faster rate compared to the same peptide segment within the protein in its native state. These differences in exchange rates, when combined with protein sequence analysis and homology modeling, can provide key insights into changes in local protein dynamics due to structural perturbations at peptide resolution.

MATERIALS AND METHODS

Sample Preparation

Monoclonal antibody mAb1 (IgG2, calculated *pI* of 8.7) was obtained from the purification group within Amgen, Inc. The purified mAb1 bulk material at 150 mg/mL was stored frozen in a mildly acidic buffer. The purified mAb1 solution was thawed and buffer exchanged into 20 mM acetic acid (pH 5.0 @ 20C) using Slide-A-Lyzer™ Dialysis Cassettes (Life Technologies, Grand Island, NY) and then diluted to 20 mg/mL using the same buffer. After dilution, a portion of mAb1 bulk material was stored in 125 mL media bottles and kept at 2° -8°C for two years for use in assessing the properties of mAb1 dimer species that were present after long-term storage. The remaining material was used to generate thermal stressed induced dimer species. Thermal-induced dimer material was prepared by placing 30 mL aliquots of

mAb1 bulk material, stored in 50 mL Falcon™ conical centrifuge tubes, in a VWR Gravity Convection Incubator (VWR, Radnor, PA) set to 50°C for 3 days. Additionally, 50 µL aliquots of the original mAb1 purified bulk material (at 150 mg/mL) were stored frozen at -70°C in 0.5 mL Eppendorf® Snap-Cap Microcentrifuge tubes (Fisher Scientific, Pittsburgh, PA) for use as a reference standard.

Analytical size exclusion chromatography (SEC)

The relative size distribution of mAb monomers and dimers were determined by SEC using a Waters H-Class UHPLC System (Waters Corporation, Milford, Massachusetts) equipped with an ultraviolet (UV) diode array detector. For each sample, 60 µg of protein was injected onto a gel filtration column (ACQUITY UPLC PrST SEC Column, 200Å, 1.7 µm, 4.6 mm X 300 mm; Waters Corporation, Milford, Massachusetts) equilibrated in a running buffer mobile phase comprised of 100 mM sodium phosphate, 250 mM NaCl at pH 6.8 at a flow rate of 0.4 mL/min. Chromeleon® 7.2 Chromatography Data System (Dionex, Sunnyvale, California) was used to analyze results and peak integration was calculated using the UV absorbance of 280 nm. Reference standard mAb solutions were injected in triplicate at the beginning and end of each sequence to determine the SEC assay variability.

Protein fractionation using SEC

Monomer and dimer samples of mAb1 were purified via using an ÄKTAexplorer 100 FPLC instrument equipped with a fraction collector (GE Healthcare Bio-Sciences, Pittsburgh, PA). Five mL aliquots of each mAb1 sample type (stored at either 2° -8°C or 50°C) were injected onto a HPLC gel filtration column (TSKgel G3000SW, 250Å, 13 µm, 21 mm X 60 cm, TOSOH Bioscience LLC, King of Prussia, PA) and run at a flow rate of 2 mL/min using the same mobile phase described above for analytical SEC. The instrument was programmed to

begin collection of 1 mL fractions into a 96 deep well plate when the absorbance at 280 nm exceeded 0.20 mAU. Multiple injections were made for each mAb1 sample type to generate a sufficient supply of mAb1 monomer and dimer fractions. Upon completion of all injections, individual wells corresponding to the apexes of either monomer or dimer peaks were pooled together and concentrated to ≥ 1 mg/mL protein using Amicon Ultra-15 Centrifugal Filter Units (EMD Millipore, Billerica, MA). Monomer and dimer fractions of mAb1 were either used immediately in the phosphate containing buffer (SEC mobile phase), or were buffer exchanged to an acetate buffer containing sucrose, pH 5.0 to provide cryoprotection via dialysis as described previously, and stored frozen for future analysis. The fraction collection process resulted in four distinct samples: mAb1 dimer from long-term 2° -8°C storage, mAb1 monomer long-term 2° -8°C storage, mAb1 dimer from 50°C incubation, and mAb1 monomer from 50°C incubation.

Size Exclusion Chromatography Coupled with On Line Multi-Angle Light Scattering Detection (SEC-MALS)

SEC-MALS analysis was performed to determine the molecular weight (MW) of monomer and dimer species using an Agilent 1100 HPLC system with a TSK-GEL G3000SWxl column (5 µm particle size, 7.8 mm ID x 300 mm length; Tosoh Biosep, 08541) with a Metasaver 0.5 µm pre-column filter (Varian, A6005). The three detectors used included a Wyatt HELEOS MALS detector (light scattering), a Wyatt Optilab rEX RI detector (refractive index), and an Agilent UV detector with wavelength set at 280 nm. The SEC-MALS runs were performed at room temperature, with 100 mM sodium phosphate, 250 mM sodium chloride, pH 6.8 buffer used as the mobile phase, with a flow rate was 0.5 mL/min. Samples volumes were adjusted as necessary to ensure 300 µg of each sample were injected, without dilution, into the SEC-LS system. For

molecular weight (MW) calculation, instrument software was used with an extinction coefficient value for the mAb species of 1.5 mL/(mg*cm) at 280 nm. SEC-MALS analysis was performed in triplicate and the average and standard deviations for MW in kDa were reported.

Atomic Force Microscopy

AFM experiments were conducted with a commercial MultiMode 8 Scanning Probe Microscope and operated using ScanAsyst mode (Bruker Corporation, Billerica, MA). All measurements were performed in air using a Veeco ScanAsyst-Air Silicon Tip on Nitride cantilever (Bruker, Billerica, MA). The scan size was 500 nm, the sample size was 1024 samples/line and the scan rate was 0.4 Hz. For each sample, 20 μL of the protein solution, diluted 500x using deionized water, was incubated on a freshly cleaved mica sample disk (Bruker, Billerica, MA) for approximately 5 seconds at room temperature. After incubation, the silica surface was carefully rinsed with deionized water 10 times (100 μL each) and then dried with nitrogen gas. After drying, each sample was analyzed immediately.

Potency Assay

The potency assay for mAb-1 is a reporter gene bioassay utilizing a human erythroleukemic cell line transfected with a reporter gene construct. These cells express mAb1 antigen receptor and are activated in the presence of the antigen. Upon antigen binding to the receptor, transcription factors are activated which lead to the transcription of luciferase reporter gene. Steady-Glo® luciferase assay substrate reagent was added to the plates and read in a luminometer (EnVision). The amount of luciferase activity is directly proportional to the amount of antigen and inversely proportional to the concentration of mAb1. The biological activity of mAb1 is determined by comparing test samples to the mAb-1 reference standard. The potency

assay is performed in triplicate for each sample and the relative potency (%) and standard deviation are reported.

FcRn Binding Activity

The cell-based FcRn binding assay was developed in a competitive binding format to test the binding of the Fc moiety of monoclonal antibodies to FcRn. The assay utilized a variant of human embryonic kidney cell line, 293T (293 cells expressing SV40 large T antigen), developed internally by Amgen, which expressed FcRn on the cell surface. Varying concentrations of the mAb1 test samples and reference standard were incubated with FcRn-expressing cells and a fixed concentration of Alexa488®-labeled IgG-Fc at room temperature and at pH 6. After the incubation, the assay plate was read on a acumen® Cellista laser scanning imaging cytometer (TPP Labtech Inc, Cambridge, MA) for cell bound fluorescence. Fluorescence data from each well were recorded and analyzed using Softmax Pro version 5.4.1 (Molecular Devices, LLC, Sunnyvale, CA). After assessing similarity between response curves of test sample and reference standard, the test sample binding relative to the reference standard was determined and the results were reported as percent relative binding (% relative binding). Each sample test was performed in triplicate and the averaged % relative binding and standard deviation were reported.

Sedimentation Velocity measured by Analytical Ultracentrifugation (SV-AUC)

Sedimentation velocity was measured as an orthogonal approach to SEC for size distribution analysis using a Proteomelab XL-I analytical ultracentrifuge instrument (Beckman Coulter, Fullerton, CA). 12-mm charcoal-filled Epon 2-channel centerpieces (Beckman Coulter) and 4-hole An60 Ti analytical rotor pre-equilibrated to 20.0 °C were used. Experiments were conducted at a temperature of 20.0 °C and absorbance was recorded at 280 nm with radial scan

increment of 0.003 cm. The rotor angular velocity was 45,000 rpm. The data were analyzed by the continuous $c(s)$ distribution model in Sedfit (version 9.4) [69] using fitting parameters described previously for monoclonal antibodies [70].

Differential Scanning Calorimetry (DSC)

The thermal unfolding (or melting) temperature (Tm) was measured by differential scanning calorimetry (DSC). The energy needed to maintain the temperature between the reference cell (buffer) and the sample cell (protein) was recorded using a MicroCal VP-Capillary DSC system (GE Healthcare, Piscataway, NJ) equipped with an auto-sampler. The DSC experiments were employed using 0.5 mg/mL protein samples from 20 to 110 °C at a heating rate of 60 °C per hour. The baseline was established by subtracting the buffer-buffer scan using the Origin 7.0 software (OriginLab® Corporation, Northampton, MA). The results were presented as the change in heat capacity normalized over protein concentration.

Fourier Transform Infrared Spectroscopy (FTIR)

The overall secondary structure of mAb1 monomer and dimers were assessed by Fourier transform infrared (FTIR) spectroscopy using a Bruker Tensor™ 27 spectrometer equipped with a BioATRcell™ that is equivalent to 6 μm in path length (Bruker Corporation, Billerica, MA). The FTIR spectra were collected at room temperature with a 4 cm^{-1} interval over a range of 4000 – 800 cm^{-1} using single beam mode. Protein concentration was 1 mg/mL and each spectrum was calculated by averaging 256 consecutive scans. The buffer signal was subtracted from sample scans and the second derivative spectrum was calculated using the OPUS™ software by employing a Gaussian-Lorentzian method with a 7-point interpolation and a 9-point smoothing function.

Near and Far Ultraviolet Circular Dichroism (UV-CD)

A Jasco J-815 spectropolarimeter (Jasco Inc, Easton, MD) was used to measure near-UV circular dichroism (UV-CD) absorbance as an indication of protein tertiary structure. The CD spectrum was recorded over 240 – 340 nm using a square quartz cuvette with a 1 cm path length. All spectra were averaged over 3 scans at a 10 nm/min scanning speed and a 0.5 nm step size. Data were collected with protein samples at 0.5 mg/mL and the corresponding buffer at room temperature. The buffer signal subtraction was performed in the Spectra Manager™ software (Jasco Inc., Easton, MD) and the CD signal in mean residue ellipticity was reported. Far-UV CD applied the same conditions to measure protein secondary structure, with the exception that the absorbance spectrum was recorded over 190-240 nm.

Extrinsic Fluorescence using SYPRO® Orange Dye

Extrinsic fluorescence was applied to assess the hydrophobicity of protein samples using SYPRO® Orange dye, obtained from Invitrogen, Inc. (Carlsbad, CA), as described previously[71]. Protein samples (200 µL) were measured in 96-well microplates at 1 mg/mL with a final SYPRO® Orange concentration equivalent to 1:5000 of the original concentration. The fluorescence emission spectra were collected using a Varian Cary Eclipse Fluorescence Spectrophotometer (Varian Inc., Palo Alto, CA) equipped with a microplate reader. The excitation was 495 nm and the emission was measured from 550 to 650 nm. The slit width was set to 5 nm and the detector power was 600 volts. Three consecutive scans at a 60 nm/min scanning speed were averaged for all samples and the buffer signal was subtracted from the emission spectra.

Sodium Dodecyl Sulfate Polyacrylamide Gel Electrophoresis (SDS-PAGE)

SDS-PAGE was performed using 4-20% Tris-Glycine Gel from Bio-Rad Laboratories, Inc. (Hercules, CA). All four mAb1 samples were prepared in non-reduced and reduced forms.

For each sample, 10 µg of protein was mixed with 2x Tris-Glycine SDS sample buffer at 1:1 ratio in the presence of 15 mM iodoacetimide for non-reduced sample preparation and 25 mM dithiothreitol (DTT) for reduced sample preparation. All sample mixtures were then heated at 70^{o}C for 10 minutes. A constant voltage of 150V was applied for 40 minutes. The gel was then stained with Simply Blue Safe Stain from Life Technologies (Grand Island, NY) and destained with water.

Hydrogen/Deuterium Exchange Reactions and Mass Spectrometric Analysis (H/D-MS)

H/D-MS experiments were performed with a Twin HTS PAL liquid handling robot (LEAP Technologies, Carrboro. NC) interfaced with an Orbitrap mass spectrometer (Elite, ThermoFisher Scientific, San Jose, CA), as previously described [60, 63]. The protein concentration was adjusted with 10 mM acetate (pH 5.2) to 3 mg/mL. The H/D exchange reaction was initiated by 5-fold dilution of 3 mg/mL protein samples with 10 mM acetate in D2O (pD 5.2) as indicated for a predetermined time (10, 30 s, 1, 10 min, 1, and 4 h) at 25 °C. The exchange reaction was quenched by mixing 1:1 with ice-cold 200 mM sodium phosphate, 4 M guanidine HCl, 0.5 M Tris(2-carboxyethyl)phosphine (TCEP), pH 2.4. The quenched protein mixture was passed over a custom-packed 2 mm × 2 cm pepsin (Fisher Scientific, Pittsburgh, PA) column (Agilent Technologies, Santa Clara, CA) at a flow rate of 200 µL/min. Digested peptides were captured on a 2 mm × 1 cm C18 trap column (Waters Corporation, Milford, MA) and desalted for 3 minutes at a flow rate of 0.2 mL/min. Peptides were then separated by using a 2.1 mm × 5 cm C18 column (1.9 µm Hypersil Gold; Thermo Fisher Scientific, Waltham, MA) with a 9.5 minute linear gradient of 5–40 % acetonitrile in 0.1% formic acid at a flow rate of 0.2 mL/min. Protein digestion and peptide separation were carried out in thermal chamber

maintained at 1°C to reduce back exchange. LC-MS data were acquired with a mass resolving power of 120,000 for ions of m/z 400. Each experiment was performed in duplicate to provide an estimate of variation.

Tandem mass spectrometry (MS/MS) experiments were performed under the same conditions as described above. Product-ion spectra were acquired in a data-dependent mode, and the 10 most abundant ions were selected for product-ion analysis. All data were processed with the software MassAnalyzer[62] for the peptide identification and the deuterium level calculation. Approximately 500 peptides were analyzed with sequence coverage of at least 97% for all mAb1 polypeptide chains. All H/D-MS data were normalized to 100% deuterium incorporation and the percent deuterium incorporation was plotted against labeling time in log scale with Prism v 6.02 (Graphpad Software, La Jolla, CA). See Zhang, et al (manuscript in preparation) for a more detailed explanation of the H/D-MS protocol.

Limited Proteolysis by FabRICATOR® Enzyme

Approximately 60 µg of each sample was digested in 30 µL of 10 mM acetate, pH 5.2 containing 60 units of FabRICATOR enzyme. The reaction was incubated at 37°C overnight. For reduced samples, the digested material was treated with a buffer containing 4 M Guanidine-HCl, 50 mM Tris, pH 8.3, with 50 mM DTT. Reduced and non-reduced digests were directly separated by reverse phase chromatography with a BEH Phenyl 2.1 X 150 mm column (Waters Corporation, Milford, Massachusetts) and the mass measurements were obtained in-line using a Waters Premier Q-Tof mass spectrometer.

Disulfide peptide mapping with mass spectrometry

The mAb1 samples were denatured by diluting 33 µL of 3 mg/mL proteins in 90 µL of 8 M Guanidine-HCl, 10 mM N-Ethylmaleimide with 100 mM sodium acetate, pH 5.2, and incubated

at 37 C for 3 hours. The mixture was then diluted with 325 µL of 4 M urea, 20 mM hydroxylamine, 100 mM Tris, pH 7.0, and Lys-C was added to the mixture to achieve an enzyme to substrate ratio of 1:20. To prepare reduced digested samples, 200 µL of each digests were added with 4 µL of 0.5 M TCEP solution and incubated at room temperature for 30 min. The reduced and non-reduced Lys-C digests were analyzed by reversed phase HPLC with mass spectrometry using a Waters Acquity UPLC with an Orbitrap mass spectrometer (Elite, ThermoFisher Scientific, San Jose, CA). Approximately, 30 µg of protein digest was injected onto a Waters Acquity UPLC BEH300 C4 2.1 X 150 mm column. Mobile phase A was 0.1 % TFA in water and mobile phase B was 0.1% TFA in 90% acetonitrile. The column was equilibrated with 2% B using a flow rate of 0.2 mL/min. After sample injection, the column was washed with 2% mobile phase B for 5 minutes. A linear gradient to 20% mobile phase B over 35 minutes was applied. This was followed by another linear gradient of 20 to 40% B over next 80 minutes.

mAb1 IgG2 Three-Dimensional Homology Modeling

To illustrate the peptides showing conformational differences by H/D-MS analysis, the recombinant mAb1 IgG2 amino acid sequence was modeled against the known structure of a full-length human antibody IgG1 (Protein Data Bank entry 1HZH)[72] to create a molecular model representative of the mAb1 structure. Sequence alignments focused solely on the highly conserved (>96%) constant regions of the heavy chain. Three-dimensional modeling was performed using the Antibody Modeler component of Molecular Operating Environment software (Chemical Computing Group, Montreal, Quebec, Canada), and the final three-dimensional homology model highlighting the structural features of interest was produced using the PyMOL Molecular Graphics System (DeLano Scientific, San Carlos, CA).

RESULTS

Size distribution analysis of monomer and dimer species

A schematic overview of the process employed to purify monomer and dimer samples from mAb1 bulk material is given in Figure 3. Representative analytical SEC chromatograms for mAb1 material, before and after purification by SEC fractionation, are shown in Figure 4. Thermal incubation of mAb1 bulk solution at 50°C for 3 days resulted in a 4.5% increase in dimer peak area relative to the mAb1 bulk solution stored at 2° -8°C for 2 years (1% vs. 5.5%). A small decrease in total peak area (6.1%) was observed for the thermal incubated sample compared to the sample stored at 2°C-8°C for 2 years. Reference standard injections of the mAb1 purified bulk material showed variability for the SEC method was only ± 0.3%, suggesting that, other than possible sample handling error, the decrease in peak area for the thermally incubated protein solution could be caused by formation of mAb aggregates or particles too large for detection by the SEC method. In other words, this result suggests that in addition to dimer formation, some larger, insoluble aggregates were formed which could not pass through the SEC column. Total peak area differences were also observed for the fractionated dimer and monomer samples, but these differences are likely the result of differences in protein load due to the varying concentrations of protein fractions after collection. SEC fractionation of mab1 bulk material both before and after thermal incubation resulted in monomer and dimer fractions that contained greater than 80% peak area for each respective species. Dimer fractions, regardless of the condition by which they were generated, retained a certain portion of monomer, and thus were enriched in dimer but not completely purified. It is unclear whether the monomer present in the dimer fractions is a result of co-purification or due to disassociation of dimer upon purification.

The monomer and dimer fractions collected from mAb1 bulk material stored at 2° -8°C for 2 years and mAb1 bulk material incubated at 50°C for 3 days were used for all subsequent characterization work. For simplicity in nomenclature, monomer and dimer fractions collected from mAb1 bulk stored at 2° -8°C for 2 years will be referred to as "native monomer" and "native dimer", respectively, in all subsequent discussions. Likewise, monomer and dimer fractions collected after thermal incubation at 50°C for 3 days will be denoted "thermal monomer" and "thermal dimer". The entire process, outlined in Figure 3, was repeated as required to generate sufficient material for additional analysis.

Size Exclusion Chromatography coupled with on-line Multi-Angle Light Scattering (SEC-MALS) was used to confirm peaks eluting by SEC corresponded to the expected mass of mAb-1 monomer and dimer (~150 and ~300 kDa, respectively) (Table 2). Measurements were performed in triplicate for each sample to assess variability. While SEC-MALS is effective at distinguishing monomer from dimer species, it is not sensitive enough to distinguish potential mass differences between the native dimer versus thermal dimer.

Sedimentation Velocity measurements by Analytical Ultracentrifugation (SV-AUC) was performed as an orthogonal approach to SEC for measuring size-distribution. Results for the monomer and dimer fractions are shown in Figure 5 as continuous c(S) distributions. Although SV-AUC was able to distinguish the monomer species (S=6.4) from the thermal dimer (S=9.32) and native dimer (S=9.26), no meaningful observations can be made with regard to differences between the two dimer types. No other species, either larger aggregates or protein fragments, were detected by SV-AUC. These results suggest that the apparent loss of total peak area by SEC for the thermal incubated mAb1 bulk material is attributable (1) formation of aggregates too

large to be seen by SV-AUC, or (2) to some other type of error, rather than a loss of protein aggregates too large for SEC analysis.

Biophysical and Functional Characterization of Dimer Species

Representative images obtained by atomic force microscopy (AFM), used to observe the spatial orientation of the native monomer relative to the native dimer and thermal dimer, are shown in Figure 6. AFM was able to show qualitative differences in the spatial orientation of monomer species from dimer species, as well as between the thermal dimer from the native dimer. The AFM image of the thermal monomer was similar to native monomer by AFM (data not shown). The AFM image of the thermal dimer shows closer association between the monomer units than does the native dimer, which suggests more contact points, and perhaps stronger intermolecular interactions, are forming upon thermal stress formation of dimers.

Potency and FcRn binding, used to gauge the impacts of the dimer formation on biological activity of mAb1, were assessed for monomer, native dimer and thermal dimer. The results are shown in Table 3. Both the native and thermal mAb1 dimer species were found to have significantly reduced potency (49% and 28%, respectively) compared to the native monomer control, suggesting the Fab domain is unable to bind its target in both cases. The native dimer exhibited an increase in FcRn binding relative to the monomer control (128% versus 99%), which is potentially indicative of increased avidity caused by multivalent binding of Fc portions of mAb1 native dimer species to the FcRn receptors expressed on the cell surfaces. Similar results have been reported in the literature for other IgG mAb oligomers [73-76]. It is of note, that unlike the native dimer, the thermal dimer showed a reduced ability to bind FcRn

receptors (44%) compared to the monomer control (99%), suggesting that the Fc regions have altered structures that affect receptor binding.

Differential Scanning Calorimetry (DSC) analysis was performed to assess thermal stability of mAb1 monomer and dimer fractions. Interestingly, no differences were detected in thermal melting behavior for any of the samples tested. Only one transition midpoint (T_m) of thermal unfolding was observed, and the average T_m value based on duplicate runs was 75.2°C +/- 0.3°C. Representative DSC curves are shown in Figure 7.

Several spectroscopic based techniques were employed to detect possible structural differences between monomer, native dimer and thermal dimer species (Figure 8). Secondary structure analysis of monomer and dimer species was assessed using far-UV CD (Figure 8A) and FT-IR (Figure 8C) spectroscopy, and no significant differences between monomer and dimer, between monomer types, or dimer types were observed using these techniques. Likewise, near-UV CD (Figure 8B) proved to be insufficient mean of identifying potential tertiary structural differences between the monomer and dimer species. Extrinsic fluorescence results using SYPRO® Orange dye are shown in Figure 8D. A large increase in fluorescent signal intensity for the thermal dimer compared to the other three samples was observed. Since it has been demonstrated that SYPRO® Orange dye only fluoresces in hydrophobic environments [51, 52, 77, 78], these results indicate solvent exposed hydrophobic residues are relatively more present, and that thermal dimer samples thus undergo conformational changes or associations leading to exposure of more hydrophobic surfaces compared to both monomer types or native dimer.

SDS-PAGE was performed under both reducing and non-reducing conditions to understand the nature of bonding between dimer species. Reduced and non-reduced SDS-PAGE results are shown in Figure 9. Both types of dimer showed a mixture of covalent and non-

covalent associations, but the thermal dimer species have a more abundant population of covalent species compared to the native dimer sample, as evidenced by the apparent disassociation of native dimer under the denaturing conditions of the non-reducing SDS-PAGE gel. Both dimer types reduce to form bands corresponding to heavy and light chains upon the addition of the reducing agent, as expected, indicating that the formation of these dimer species likely involve disulfide bond rearrangements. The thermal dimer, however, showed a small amount of protein that remained as higher MW species, even after reduction, by SDS PAGE suggesting (1) incomplete reducing conditions, or (2) the formation of non-disulfide, covalent cross-linked dimers.

Understanding the mechanisms of dimer formation

Understanding the mechanism of dimer formation began by attempting to identify the specific regions of the mAb1 structure that contain induced conformational perturbations in mA1 dimer fractions using hydrogen-deuterium exchange mass spectrometry (H/D-MS). In order to establish a baseline for comparison of H/D-MS results, H/D-MS was first performed for the mAb1 native monomer sample, assuming that it closely represents the native conformation of mAb1. Duplicate H/D exchange rate measurements were made for more than 500 peptic peptides, accounting for 97% of the entire mAb1 amino acid sequence, at time-points ranging from 10 seconds to 4 hours (data not shown). Interestingly, the only peptide segments that were not recovered by H/D-MS analysis was an area of the protein that corresponds to the hinge region, which contains 4 inter-chain disulfide bonds that link the two heavy chains together. Incomplete reduction of these disulfide bonds may explain the lack of recovery for this portion of the sequence (data not shown).

The H/D-MS experiments were repeated, in duplicate, for the native dimer, the thermal dimer, and the thermal monomer, and the deuterium incorporation as a function of time for each peptide was compared to the matching peptides from the native monomer. Statistical significance was determined by applying a two-way ANOVA between consecutive time points ($p < 0.05$) (data not shown; see Zhang, et al, manuscript in preparation). Differences in deuterium incorporation were not observed for any of the peptic peptides between the native monomer and thermal monomer or between the native monomer and native dimer (data not shown: see Zhang, et al, manuscript in preparation). Compared to the native monomer, H/D-MS was able to detect four peptic peptides with faster deuterium incorporation rates for the thermal dimer, as shown in Figure 10A-D. The peptic peptides with faster deuterium incorporation rates in the thermal dimer sample correspond to the region of mAb1 sequence covering residues at positions 235-255 and 313-342, which are adjacent to the hinge region and consist of anti-parallel beta sheets. Interestingly, these peptides also contain the cysteine residues responsible for the formation of the intramolecular disulfide bond in the C_H2 domain. Panels A-D in Figure 10 show the deuterium uptake rate curves for the four peptic peptides from the thermal dimer sample compared to the same peptic peptides from the native monomer, and each peptic peptide is shown with its corresponding portion of the mAb1 sequence. Panels E-F in Figure 10 show the deuterium rate curves for the native dimer compared to the native monomer for the same peptic peptides shown in Figure 10A-D. It is worth noting that the peptic peptides from the thermal dimer sample that showed the largest differences in deuterium incorporation rates (the peptic peptides containing residues at positions 246-255 and 313-342) each contain one cysteine residue that together form the intramolecular disulfide bond within the C_H2 domain.

A 3D homology model of mAb1, as shown in Figure 11, was created to highlight (in red) the portions of the thermal dimer showing faster rates of deuterium incorporation by H/D-MS analysis. The 3D homology model for the entire mAb1 molecule is shown in Figure 11A. The portions of mAb1 showing increased structural flexibility were localized to the C_H2 domain, just below the hinge region, as shown in the zoomed-in view of the 3D model Figure 11B. The cysteine residues that form the intramolecular disulfide bond and the N-glycans are highlighted in cyan and blue, respectively. Portions of the mAb1 molecule that showed no differences in deuterium incorporation are colored gray.

To better understand these results, the thermal dimer was analyzed in greater detail. The 3D homology model for mAb1 shows that the regions with increased flexibility in the thermal dimer sample surround the intramolecular disulfide bond located in the C_H2 domain. The SDS-PAGE analysis suggested that significant amounts of thermal dimers are disulfide linked. On the basis of the SDS-PAGE and H/D-MS data, it was hypothesized that mAb1 thermal dimer formation involves the intramolecular disulfide bond of the C_H2 domain. This possibility was examined with the thermal dimer by several mass spectrometry techniques.

First, limited proteolysis was performed using FabRICATOR enzyme. FabRICATOR enzyme is a protease with one specific cleavage site in all human IgG subclasses below the hinge region. Enzymatic digestion of an IgG with FabRICATOR produces a divalent Fab (Fab'2) fragment and two half-Fc (Fc/2) fragments[79]. Reduction of the Fab'2 fragment results in two light chain (LC) fragments and two Fd fragments. Reversed phase liquid chromatography followed by mass analysis was performed on both non-reduced and reduced digests of mAb1 monomer and dimer fractions, shown in Figure 12. Figure 12A shows the reversed phase chromatograms for the native monomer and native dimer samples under reducing and non-

reducing conditions after FabRICATOR digestion. Under non-reducing conditions, the native monomer and native dimer samples (shown in red and blue, respectively) follow expected reversed phase chromatogram profiles; two major peaks with masses of 25232.5 Da and 95936 Da, corresponding to the Fc/2 (Peak 1) and Fab'2 (Peak 5) fragments, respectively. Upon reduction of the native monomer and native dimer FabRICATOR fragments (shown by the black and cyan colored traces, respectively), the Fab'2 is reduced to Fd (Peak 7) and LC fragments (Peak 3). The Fd fragments consist of the V_H, C_H1 and hinge portions of the heavy chains. A significant retention time shift is observed between the non-reduced and reduced Fc/2 fragments due to the significant structural change that occurs upon reduction of the intramolecular disulfide bonds located within the C_H2 and C_H3 domains. A mass increase of 4.5 Da is observed in the peak corresponding to the reduced Fc/2 fragments (Peak 2), which corresponds to the reduction of all four cysteine residues in each Fc/2.

Figure 12B shows the reversed phase chromatograms resulting from FabRICATOR digestion under non-reducing and reducing conditions for the thermal monomer and thermal dimer samples. The thermal monomer showed comparable profiles to the native monomer and native dimer samples under both non-reducing and reducing conditions. Under non-reducing conditions, the thermal dimer (blue trace) shows peaks corresponding to Fc/2 (Peak 1) and Fab'2 (Peak 5) fragments, albeit with much lower intensities compared to the thermal monomer sample (red trace). Interestingly, the thermal dimer sample also produced a shoulder peak next to the Fab'2 peak (Peak 4) that was too large for mass determination. Upon reduction, as shown by the cyan-colored trace in Figure 12B, this shoulder peak disappears and a peak corresponding to the mass of a single HC (49770 Da, Peak 6) is observed alongside the reduced Fc/2 (Peak 2), LC

(Peak 3) and Fd (Peak 7). Thus, it is inferred that the shoulder peak represents mAb1 material that was resistant to FabRICATOR cleavage.

The FabRICATOR cleavage site was confirmed by mass analysis for mAb1 monomer (data not shown) to be located in the hinge region at a glycine residue at position 231 of the mAb1 sequence. The 3D model of the mAb1 C_H2 domain structure is shown again in Figure 13A, highlighting in red the peptides where conformational flexibility was detected in the thermal dimer sample by H/D-MS analysis as well as the cleavage site, highlighted in green. The FabRICATOR cleavage site is located directly upstream from the regions that H/D-MS indicated having conformational flexibility. Indeed, a very small difference in deuterium incorporation rate was also observed for a five peptide long peptic peptide (covering residues 229-234) containing the FabRICATOR cleavage site (Figure 13C). Thus, it is proposed that the increase in conformational flexibility in the C_H2 domain observed by H/D-MS is responsible for preventing the full FabRICATOR enzyme digestion of mAb1 thermal dimer species.

LC/MS disulfide peptide mapping was employed to detect the differences in disulfide bonding among the mAb1 monomer or dimer samples. The profiles of reduced and non-reduced peptide map mass spectra for the mAb1 fractions studied (native monomer, native dimer, thermal monomer and thermal dimer) are shown in Figure 14. The four species produced comparable LC/MS peptide map results under both reducing and non-reducing conditions. All expected peptides were recovered and no new peptides were detected in any of the four samples. In sum, the disulfide peptide mapping revealed no evidence of a change in disulfide bonding patterns from the native mAb1 structure for either type of dimer. Although some peptides do show minor differences in peak heights, this is likely attributable to variability in digestion efficiency, variability of the chromatography method itself, or a combination thereof. These results appear

to be inconsistent with the SDS-PAGE results, which implicated disulfide bonding as a possible mechanism of dimer formation. Additionally, the H/D-MS data is highly suggestive of the C_H2 domain intramolecular disulfide bond as having a role in dimer formation. Limited proteolysis using FabRICATOR enzyme also indicated that the C_H2 has an altered structure in the thermal dimer sample that prevents full enzymatic cleavage. These apparent inconsistencies will be addressed in the following discussion.

DISCUSSION AND CONCLUSIONS

Summary of Findings

The analytical characterization of the two IgG2 mAb dimer types, one formed after long-term storage at 2°-8°C, the other formed upon thermal incubation, provided meaningful insights into the nature of dimer formation for this mAb. Two orthogonal methods used to assess protein size distribution, SEC-MALS and AUC, were able to differentiate monomer from dimer species, but could not demonstrate meaningful differences in hydrodynamic size between native and thermal dimers. AFM analysis showed qualitative differences in the physical orientation between the monomers, native dimers and thermal dimers. Interestingly, several other lower resolution biophysical techniques, including DSC, FT-IR and CD were unable to detect differences in the structural integrity for any of the IgG2 mAb samples.

The mAb1 native dimer is mostly disassociated upon exposure to the denaturant (in this case SDS). The mAb1 native dimer fraction contained greater than 90% dimer species via SEC, but showed a much fainter band corresponding to the dimer oligomer in the non-reducing SDS-PAGE gel. For the thermal dimer sample, approximately 82% of species being dimer by SEC with a higher percentage (compared to the native dimer) being covalently linked as observed qualitatively by SDS-PAGE. The mAb1 native dimer was fully reducible to HC and LC fragments with the addition of DTT. The biological activity results suggest that the Fab region has a significantly reduced ability to bind to its antigen target, however, the Fc remains biological active and presumably structurally intact. AFM shows that native dimer is comprised of individual monomeric units that are closely associated but not overlapping. H/D -MS results were unable to explain the reduction in potency for mAb1 native dimer species because no differences in structural flexibility were identified in the Fab portion of mAb1 native dimer

compared to the monomer control. It is presumed that the interactions between Fab domains at the dimer interface, which result in a reduced binding affinity for the antigen, involve surface exposed, flexible peptide segments where deuterium incorporation is relatively rapid or that any structural differences between the native dimer and monomer are too subtle even for detection by H/D-MS.

Similar to the native dimer, the thermal dimer samples showed potency assay results that indicated a reduced ability of the Fab to bind its antigen target. Unlike the native dimer, however, the thermal dimer showed a reduction in FcRn binding ability, suggesting the Fc domain of these species are also compromised. Again, AFM results support these findings as they show a thermal dimer with two more closely associated monomer units. Extrinsic fluorescence with SYPRO® Orange was able to detect the presence of increased surface hydrophobic patches. This result indicates more structural differences exist between the thermal dimer and the native dimer, as compared to the native monomer and thermal monomer species. SDS-PAGE analysis revealed that, compared to the native dimer species, a larger portion of mAb1 thermal dimer species are covalently linked. Most of the thermal dimer samples were reducible to HC and LC chains, suggesting disulfide bonds play a role in thermal dimer formation. The mAb1 thermal dimer sample also showed a small amount of higher MW species, even after reduction, which suggests the possibility of the incomplete reducing conditions, or that the mAb1 thermal dimer sample contained some portion of dimer with non-disulfide covalent cross-linkages.

More detailed analysis of the thermal dimer species using mass spectrometry based methods revealed additional details about the possible cause of dimer formation. H/D-MS was able to provide insight into the parts of mAb1 with induced conformational differences by

probing the entire structure. Similar to the native dimer, even though there was a significant reduction in potency, no differences in deuterium uptake were observed in the Fab domain for the thermal dimer. H/D-MS did, however, implicate the C_H2 domain as a potential interface for dimer formation, with limited proteolysis using FabRICATOR enzyme provided further evidence that mAb1 thermal dimer involved interactions of the C_H2 domains at the dimer interface. Finally, disulfide peptide mapping mass spectrometry showed that even though all prior results implicated the involvement of disulfide bonds in the formation of the thermal dimer, there was no indication of deviations from native disulfide bonding patterns.

Based on the data presented here, it is reasonable to conclude that the mechanisms of dimer formation in mAb1 material involve many types of covalent and non-covalent protein-protein interactions under both types of storage conditions assessed. Indeed, substantial quantities of both native and thermal dimer were readily disassociated by the denaturing conditions of the SDS-PAGE gel. Like the thermal dimer, the native dimer also showed evidence of disulfide linked covalent bonding by SDS-PAGE, but those results could not be explained by any conformational differences by H/D-MS analysis.

However, two potential mechanisms of mAb1 dimer formation, demonstrated in Figure 15, are proposed to help explain the results from this work. For mAb1 material subjected to thermal incubation, we suggest one possible mechanism of dimer formation, supported by the data, that occurs via domain swapping of intramolecular C_H2 disulfide bonds to form a covalent disulfide linkage between two mAb1 monomers (Figure 15A). Although there is little direct evidence explaining the formation of the native dimer in mAb1 material stored long term at 2° - 8°C, indirect evidence is suggestive of a mixture of covalent and non-covalent surface interactions at or near the Fab domains (Figure 15B). In both cases, dimer species retain a

substantial level of the native mAb1 monomer structure as evidenced by the CD, FTIR and H/D-MS results.

Since, for the mAb1 thermal dimer, all of the expected peptides and disulfide-linked peptides were recovered, and there was no evidence of unbound cysteine residues and or scrambled disulfide bonds, the disulfide peptide mapping results appear to contradict the SDS-PAGE and FabRICATOR results that implicated increased covalent disulfide bonding in the thermal dimer sample compared to the native monomer and native dimer samples. Recently, Iacob et al observed a similar phenomena for a different IgG mAb [30]. The authors invoked the concept of domain swapping dimerization, previously reported as aggregation mechanisms for several protein types, including an IgG1 [80-84], to explain the discrepancies that were observed between SDS-PAGE and LC/MS disulfide peptide map results. In short, domain swapping occurs when a covalent or non-covalent interaction, native to one protein domain, is disrupted and the same interaction is reformed between two protein monomers at the same position on a neighboring, but identical, domain resulting in the formation of a dimer aggregate.

The evidence presented in this thesis suggests that a similar mechanism of domain swapping dimer formation occurs under thermal stress conditions for mAb1. It is proposed that during thermal incubation of mAb1 solution, the intramolecular disulfide bond of the C_H2 domain disassociates in several mAb1 monomers within the same timescale. Subsequently, the unpaired cysteine residues form a new disulfide bond, but intermolecularly, with the same unpaired cysteine residue on two adjacent mAb1 monomers in solution. Looking back to the H/D-MS results that identified the cysteine containing peptides with increased flexibility in the C_H2 domain as an example, it is known that the intramolecular disulfide bond is formed between the cysteine residue contained within positions 246-255 and the cysteine residue contained

within positions 313-342 of the mAb1 sequence for the native mAb1 molecule. The formation of the thermal dimer via domain swapping would result from the pairing of same cysteine residues, but between two monomers, such that the cysteine (246-255) on Monomer 1 pairs with the cysteine (313-342) on Monomer 2, or conversely, between the cysteine (246-255) on Monomer 2 and cysteine (313-342) on Monomer 1. The apparent inconsistencies arising from the disulfide peptide mapping results are thus explained: a difference between the intermolecular disulfide bonds of the thermal mAb1 dimer compared to the native mAb1 intramolecular disulfide bonds would not be observed because the same overall cysteine-cysteine connectivity is maintained after proteolysis by the enzyme.

The result of this domain swapping dimerization is that most of the higher order structure is maintained, and very sensitive and specific techniques are needed to detect the resulting minor conformational changes, as was demonstrated from the SYPRO® Orange Fluorescence and H/D-MS results. This helps to explain why methods measuring protein secondary and tertiary structure by CD and FTIR were unable to detect structural differences between any of the samples: structural measurements by such techniques provide globally averaged values that overwhelm any the relatively minor spectral contributions from the altered structure. The H/D-MS results were only able to show increases in conformational flexibility in peptides localized to the C_H2 domain in the thermal dimer sample, specifically in peptides containing the cysteine residues that form an intramolecular disulfide bond within the C_H2 domain. The limited proteolysis via FabRICATOR enzyme resulted in incomplete digestion ofmAb1 thermal dimer species, which can be explained by the blocking of the cleavage site by the closely interacting disulfide linked Fc regions of the two mAb1 molecules.

Further evidence supporting the models of aggregation mechanisms for mAb1 native and thermal dimer samples resides in the AFM, FcRn binding and potency results. Both the native and thermal dimer species showed reduced potency, suggesting both conformations have Fab orientations that prevent binding to the surface expressed antigen. The potency of the native dimer was reduced by approximately 50% relative to the mAb1 control. The thermal dimer was even less potent (28%). It is suggested that the Fab regions for these two dimer types are interacting, covalently or non-covalently, via solvent-exposed residues in such a way that the CDRs are prevented from binding to the antigen receptors.

The native dimer showed an increase in FcRn binding compared to control while the thermal dimer showed significantly reduced FcRn binding. It has been demonstrated that the structural integrity of the C_H2 domain plays a key role in FcRn binding[85-87]. If indeed the thermal dimer is formed via C_H2 domain disulfide swapping, then the lack of proper FcRn binding is expected. Likewise, if the native dimer is mostly the result of interacting Fab regions, it is reasonable to assume that the Fc portions of each monomer unit of the dimer would have sufficient freedom to bind with the cell receptor, resulting in the avidity that was observed. AFM provided representative images showing protein orientations that align with the potency and FcRn results.

Even though H/D-MS results implicated the increased flexibility the C_H2 domain, specifically around the intramolecular disulfide bond, as a contributor to formation of the thermal dimer, it is possible that other protein-protein interactions occur in this region that lead to dimer formation. Certainly, the proposed mechanism of disulfide bond domain swapping cannot account for the formation of all dimer species in the enriched thermal dimer fraction, as evidenced by the SDS-PAGE and FabRICATOR proteolysis results. SDS-PAGE results showed

the presence of a significant non-covalent dimer population, as well as possible non-disulfide covalently linked species in the thermal dimer sample. The limited proteolysis data showed that FabRICATOR enzyme was partially able to cleave the mAb1 species in the thermal dimer sample, indicating that a portion of mAb1 molecules in solution had cleavage sites that were accessible and/or sufficiently structurally intact. At this point, there is not sufficient evidence to definitively prove domain swapping as a mechanism of dimer formation in mAb1, and therefore, it is reasonable to conclude that, for mAb1 molecules, dimer species are a heterogeneous population that result from a variety of mechanisms involving covalent and non-covalent interactions.

The hinge region was not fully recovered by H/D-MS analysis, thus we can not rule out that it may also be playing a role in the formation of mAb1 dimers. For both naturally occurring and recombinant IgG2 mAbs, several interconverting isoforms that involve intermolecular disulfide bonds between the Fab arms and the hinge region have been observed [88]. Interconverting IgG2 disulfide isoforms require the breaking and reformation of disulfide bonds at the hinge region, and therefore, it is reasonable to hypothesize that some IgG2 dimers may form as a result of this naturally occurring process. Recently, Zhang et al were able to show differences in conformational flexibility by H/D-MS for different IgG2 disulfide isoforms [89]. It is possible that differences in IgG2 disulfide isoform conformational flexibility contributes to their aggregation propensity, but this is an area of study that has not been fully explored to date. Additionally, it is possible that mAb1 may contain trace levels of free sulfhydryl groups that lead to the formation of intermolecular disulfide bonded dimer species.

In a recent review, Majumdar et al showed that a potential aggregation hotspot in the C_H2 domain of IgG1 mAbs. This highly conserved sequence, FLFPPKPKDTLM, showed remarkable

similarities for increased deuterium incorporation by H/D-MS analysis for a variety of IgG mAbs from different laboratories when exposed to a variety of different stress conditions [68]. The increased conformational flexibility of this peptide segment suggests that this portion of the C_H2 domain is particularly susceptible to partial unfolding (i.e., increased local flexibility), leading to an exposure of buried hydrophobic amino acid residues, and triggering covalent and non-covalent protein aggregation. Indeed, mAb1 contains the same sequence, FLFPPKPKDTLM, at positions 235-246, and also showed increased deuterium incorporation, as shown in Figure 10A. Thus it is possible that, as with the similar reports cited by Majumdar et al, this peptide segment contributes to the dimer formation observed in mAb1 under both thermal and native storage conditions. A partial unfolding at this portion of the C_H2 domain could certainly potentially lead to solvent exposure of hydrophobic residues, which could drive protein-protein interactions between monomers due to non-covalent interactions between the hydrophobic residues of the FLFPPKPKDTLM peptide segments. Such non-covalent hydrophobic interactions could play a role in dimer formation that does not involve covalent crosslinking via disulfide bonds, and thus would be readily reversible under denaturing conditions as observed by SDS-PAGE. At the same time, it is reasonable to envision that for mAb1, covalent dimer formation via intermolecular disulfide bonds could also be mediated by increased interactions between these same solvent exposed hydrophobic regions in the C_H2 domain.

Future Work

In this study we successfully demonstrated one mechanism of mAb dimerization for one specific IgG2 mAb formed under thermal stress conditions. While this work provides meaningful

insights toward understanding the role of domain swapping via disulfide bond rearrangements in mAb aggregation, much more work must be done in order to demonstrate if any broader implications of this aggregation pathway exist. Several experiments are proposed to continue evaluating the cause of dimer formation and the role of dimer in the overall aggregation pathway.

Can domain swapping caused by disulfide bond rearrangement be demonstrated in other IgG mAbs, and under what specific environmental conditions?

At this point, the proposed mechanism of dimer formation via domain swapping caused by rearrangements of the intramolecular C_H2 domain disulfide bonds should only be understood in the context of the specific mAb IgG2 used in this research, and only under the specific stress conditions under which the dimer was generated. To date, only one other report has reported similar results for an IgG2 mAb[30]. To understand how universally applicable such a mechanism of mAb dimer formation is, various mAbs of different IgG subclasses should be studied using H/D-MS to identify the regions involved in dimer formation. A variety of environmental stress conditions, including low-pH, UV-light exposure, mechanical stress, to name a few, should be examined to see how dimer is formed under those conditions. In addition, the role of formulation with respect to pH, buffer and excipients should be factored in to such experiments.

Is it possible to block, and thus prove, the proposed mechanism of dimer formation under thermal stress conditions?

If a molecule can be introduced into the solution environment that competitively binds free cysteine residues once C_H2 disulfide bonds are reduced, it could be possible to prevent the dimer formation. One example of such an experiment would involve repeating the thermal incubation conditions leading to domain swapping via covalent disulfide bond rearrangement in the presence of N-ethylmaleimide (NEM). NEM is reactive with thiol groups and is commonly used to detect unpaired cysteine residues and block the formation of artifacts due to disulfide scrambling during non-reducing SDS-PAGE analysis[90]. Because NEM forms a highly irreversible bond with the thiol group of cysteine residues, subsequent mass analysis could used to confirm the mechanism of disulfide shuffling and potentially measure the kinetics of such a reaction under different environmental stress and formulation conditions.

Is it possible to observe the fate of dimer species in the overall aggregation pathway?

A proposed an experiment designed to study the role of dimer in the overall aggregation pathway was supported with the help of Amgen. A mAb IgG2 was successfully produced in media where the only available cysteine is ^{13}C-^{15}N labeled. As a result, all cysteine residues have a +2 Da mass shift, and the intact mAb has a mass increase of 36 Da. It is proposed, as a consequence of the mAb mass difference, that this cysteine-labeled mAb can be used a tracer in a solution of the same unlabeled mAb produced in normal media (i.e. with a normal MW). For example, dimer fractions collected from the cysteine-labeled mAb could be introduced into unlabeled mAb solution and the fate of the labeled dimer—including the formation of higher-order oligomers, remaining in solution as a dimer, or disassociating back to its monomer form—

could be observed over time and under various solution conditions. To date, the experiment remains in the planning phase.

Understanding the threshold of structural changes required to predict biological consequences of mAb aggregates.

The CD, FTIR and H/D-MS methods were unable to detect differences in Fab domain structure even though more than a 50% loss in potency was observed for both thermal and native dimer species. It was hypothesized that dimerization involves surface interactions between Fab domains that impede the mAb1 dimer from binding to the antigen receptor. However, if such interactions do not alter underlying protein secondary or tertiary structure, then it is very difficult to measure differences between conformations using the aforementioned techniques and may not be useful for predicting the biological consequences of protein aggregates that retain a significant amount of native structure.

Previously, work by Zhang et al demonstrated an ability to detect structural differences by H/D-MS analysis in the Fab regions of aggregated IgGs resulting from a different thermal stress and repeated freeze-thaw cycles, implicating portions of the HC variable domains as the interacting sites of the protein aggregates[91]. Future work should address these discrepancies by attempting to identify the minimum threshold of conformational changes that are required to be detectable by H/D-MS, and to correlate those changes back to the biological activity of the altered structural forms.

FIGURES

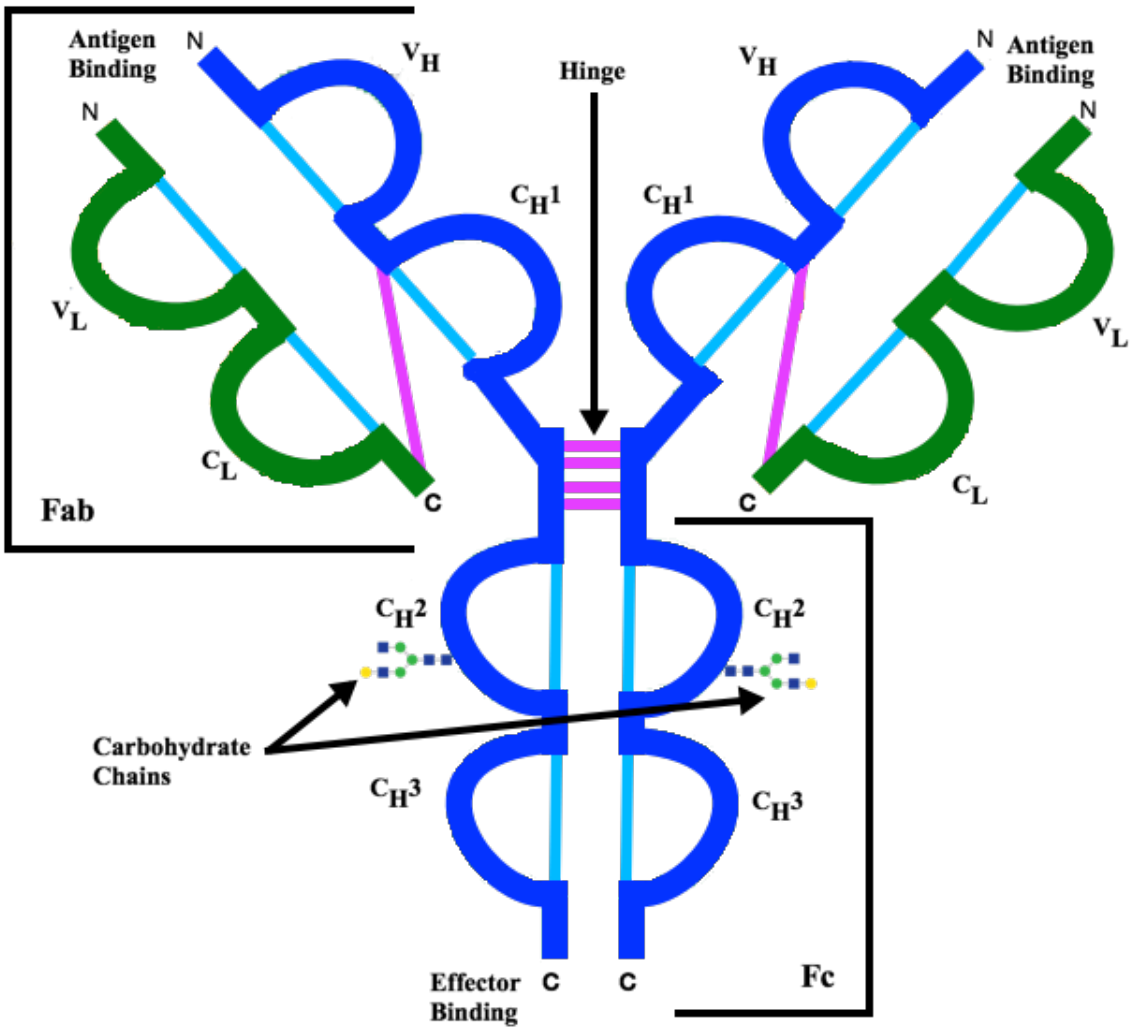

Figure 1—Two-dimensional (2D) line drawing highlighting the features of a typical IgG2 monoclonal antibody. The 2D line drawing shows the four polypeptide chains that make up the Y-shaped homodimeric mAb monomer. Heavy chains (dark blue) are covalently linked together at the hinge region by four inter-chain disulfide bonds (magenta lines). The light chains (green) are covalently linked to the each heavy chain by an inter-chain disulfide bond as well. In total, 12 globular domains (C_H2, V_L, etc.) are formed upon folding with the help of intramolecular disulfide bond (cyan lines) and other non-covalent interactions. The two Fab arms, responsible for antigen binding, contain the variable domains for the heavy (V_H) and light (V_L) chains beginning at the N-terminus. The variable domains contain highly specific amino acid sequences that form loops, known as CDRs, are responsible for binding the epitope on the antigen surface. The Fc region, located below the hinge, has a highly conserved primary sequence in human IgGs and its primary role is for effector binding that initiating immune response. A carbohydrate chain is attached to the N-glycosylation site in the C_H2 domain. The 2D figure was created using a simple drawing software program, "Paint 2 for Mac, Version 5.1.10" (TryBest Studio).

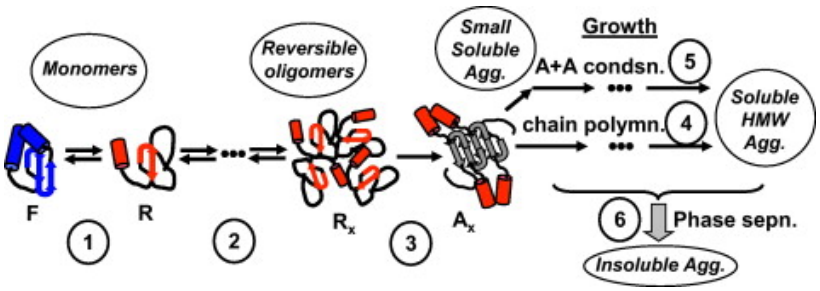

Figure 2—Schematic representation of the key steps in non-native protein aggregation. In step 1, a protein monomer in its native, folded conformation (F) may undergo a structural change that results in a partially unfolded conformation (R). (2) Reversible self-association of folded or partially unfolded monomers to form reversible oligomers containing x-number of monomer units (R_x). (3) Structural or conformational rearrangement of otherwise reversible oligomers create stabilizing intermolecular interactions that result in the formation of irreversible soluble aggregates containing x-number of monomer sub-units (A_x). Growth of the aggregate via addition of monomer subunits (4) or via interaction of multiple aggregates forms (5) may form large, high molecular weight (HMW) soluble aggregates. Growth of aggregates via phase-separation results in the formation of insoluble aggregates, such as particulates (6).
Adapted with permission from Roberts, et al, Copyright 2011, International Journal of Pharmaceutics[17].

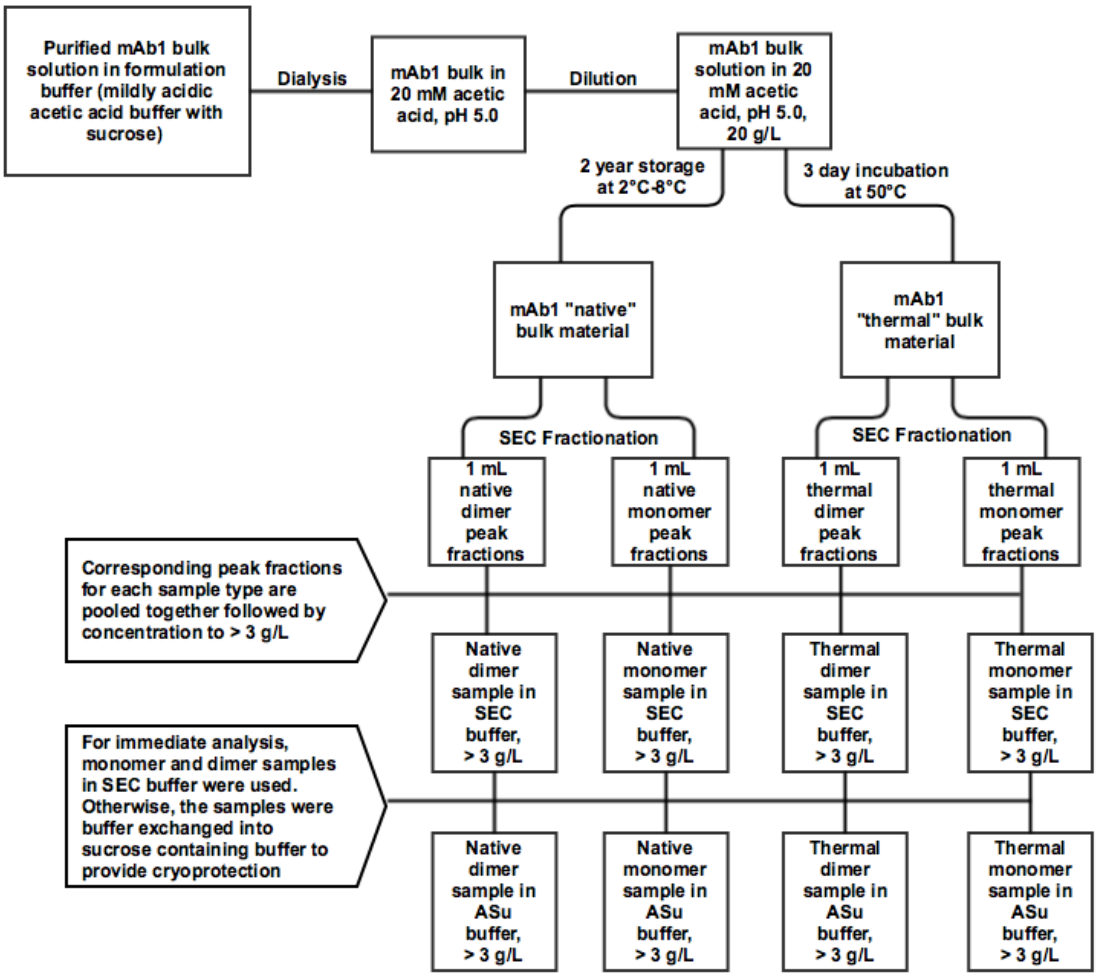

Figure 3—Schematic overview of monomer and dimer purification from mAb1 material. SEC buffer was composed of 100 mM sodium phosphate, 250 mM sodium chloride, pH 6.8. ASu buffer was composed of 20 mM acetic acid, 200 mM sucrose, pH 5.0.

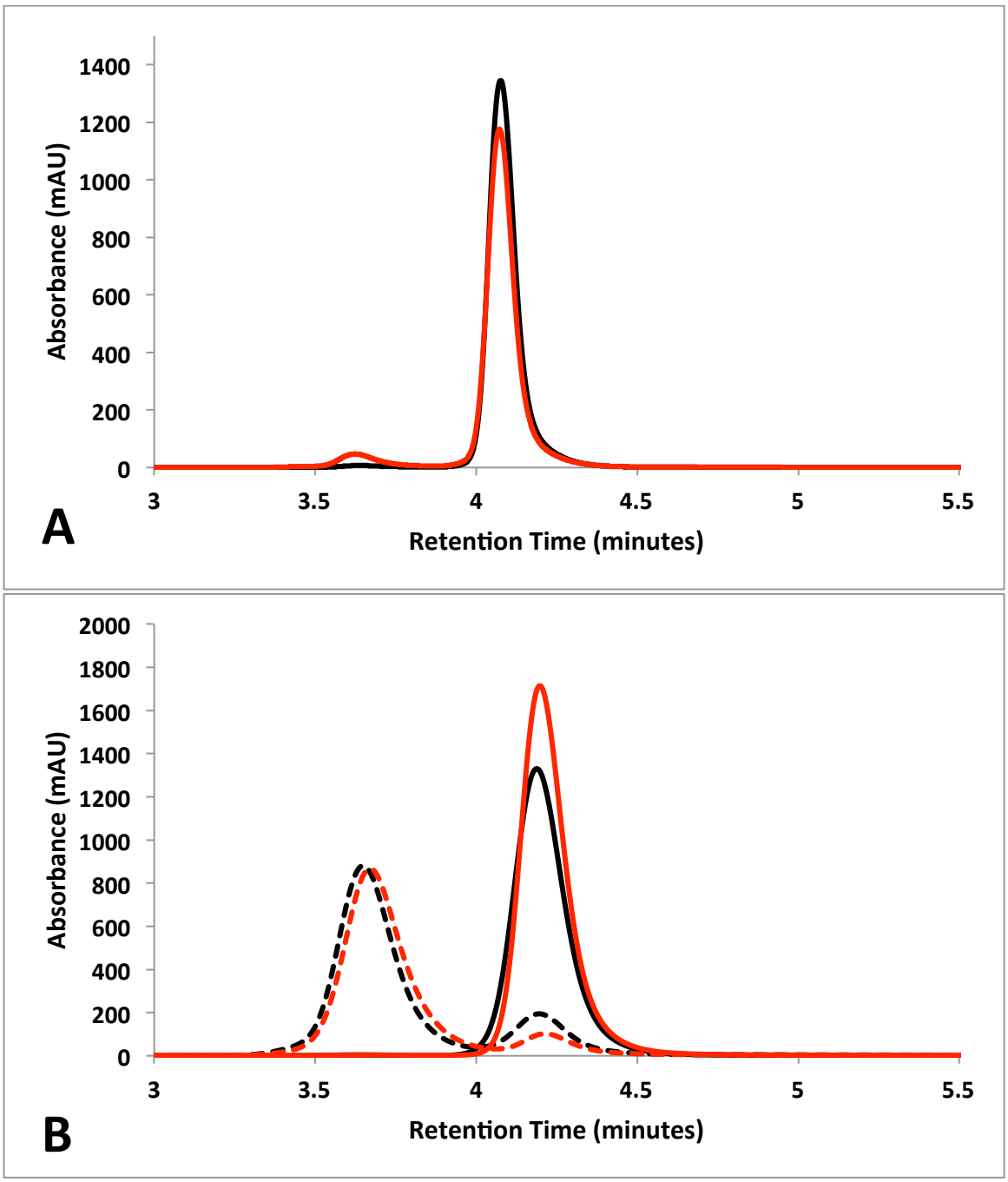

Figure 4—Representative Analytical Size Exclusion Chromatography (SEC) chromatograms for mAb1 material before (A) and after (B) purification by preparative scale SEC. Figure 1A shows results for mAb1 bulk solution after long term storage (2 years at 2°C-8°C) (black) and after thermal incubation (t=3d 50°C) (red). Figure 1B shows results for mAb1 native dimer (dashed black trace), native monomer (solid black trace), thermal dimer (dashed red trace) and thermal monomer (solid red trace). The absorbance in mAU at 280 nm is shown.

Peak Area Percentage (%)	mAb1 Bulk		mAb1 Fractions after SEC Purification			
	t=2y, 4°C	t=3d, 50°C	Native dimer	Thermal dimer	Native monomer	Thermal monomer
Dimer	1.0	5.5	91.1	82.3	0.1	0.2
Monomer	98.9	94.0	8.9	17.7	99.9	99.8

Table 1—Peak area percentages (%) by analytical SEC of dimer and monomer species in mAb1 bulk solution after long-term storage (2 years at 4°C) and after thermal incubation (3 days at 50°C), as well as native and thermal monomer and dimer fractions after SEC purification. The values listed in the table are representative of one protein fraction collection process, overviewed in Figure 3. The error of the SEC method calculated using multiple injections of a reference standard was ± 0.3%.

Sample	Molecular Weight (kDa)
Native Dimer	288 ± 1.7
Thermal Dimer	293 ± 1.6
Native Monomer	150 ± 0.8
Thermal Monomer	156 ± 0.9

Table 2—Molecular Weight (kDa) of mAb1 dimer and monomer samples determined by SEC-MALS. Each sample was analyzed in SEC mobile phase. Testing was performed in triplicate to determine standard deviations.

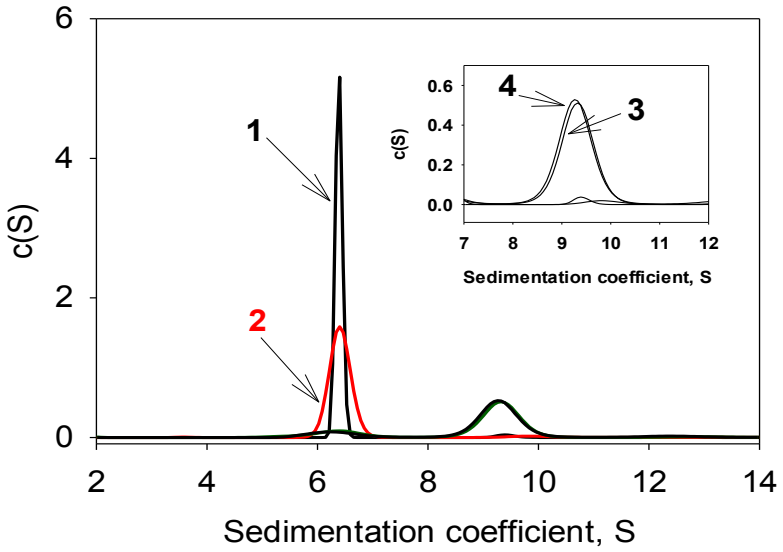

Figure 5—Size distribution by sedimentation velocity using Analytical Ultracentrifugation (AUC). Representative continuous *c*(*s*) distributions are shown for mAb1 reference standatrd (1, S=6.4), native monomer (2, S=6.4), native dimer (3, S=9.26) and thermal dimer (4, S=9.32).

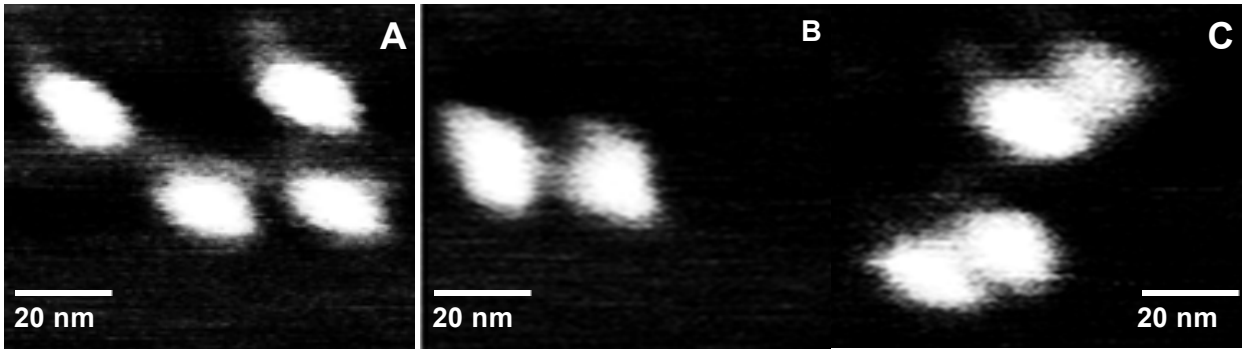

Figure 6—Representative Atomic Force Microscopy (AFM) images of mAb1 native monomer (A), native dimer (B) and thermal dimer (C).

	Native Monomer	Native Dimer	Thermal Dimer
Average Relative Potency (%)	**114 ± 13**	**49 ± 3**	**28 ± 1**
Average Relative FcRn Binding (%)	**99 ± 14**	**128 ± 8**	**44 ± 8**

Table 3—Potency and FcRn Binding results for mAb1 native monomer, native dimer and thermal dimer samples. Both potency and FcRn binding assays were performed in triplicate and the values presented in the table represent the average values and standard deviation.

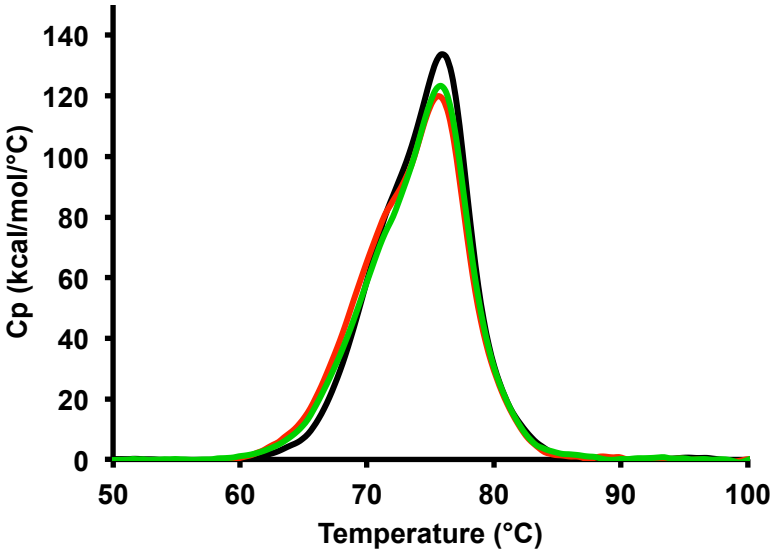

Figure 7—Protein unfolding upon temperature melting by Differential Scanning Calorimetry (DSC). Representative DSC curves are shown as plots of heat capacity (cP) versus temperature (°C) for native monomer (black trace), native dimer (red trace) and thermal dimer (green trace). Traces are normalized for protein concentration.

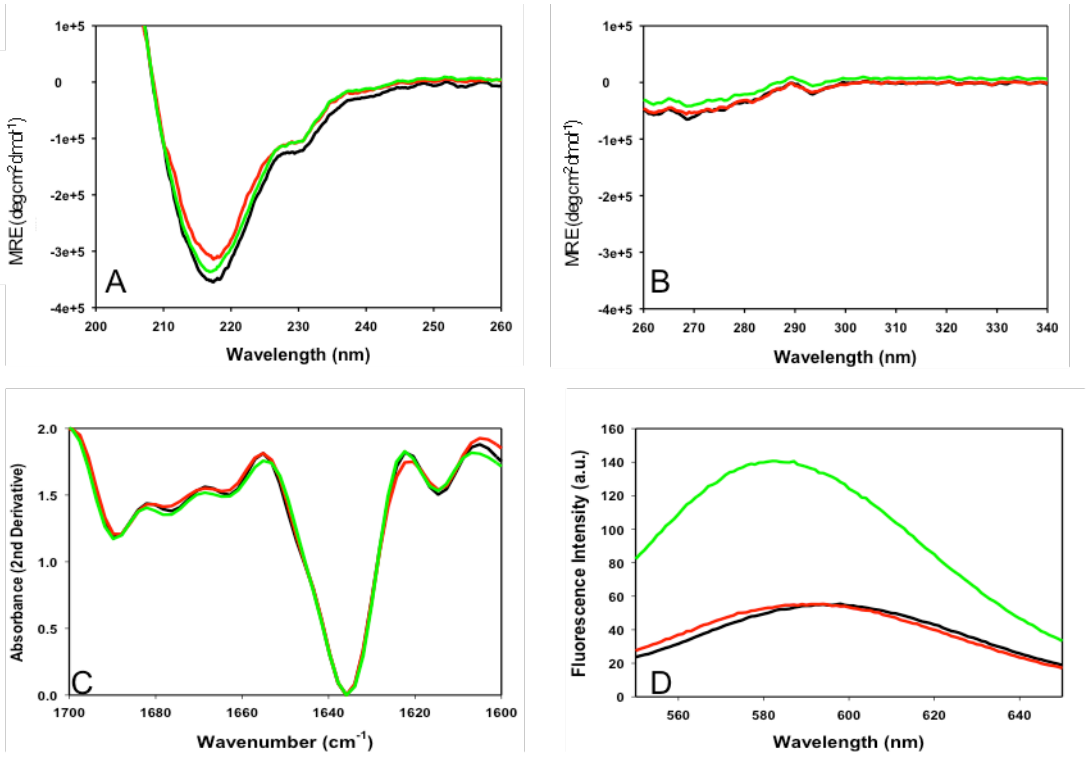

Figure 8—Representative spectra of mAb1 native monomer (black), native dimer (red) and thermal dimer (green) by Far UV-CD (A), Near UV-CD (B), FT-IR (C) and Extrinsic Fluorescence by SYPRO® Orange techniques. The CD spectra are presented as mean residue molar ellipticity. The second derivative FT-IR absorbance spectra are shown. Fluorescence intensity for the emission range resulting from excitation at 495 nm is shown.

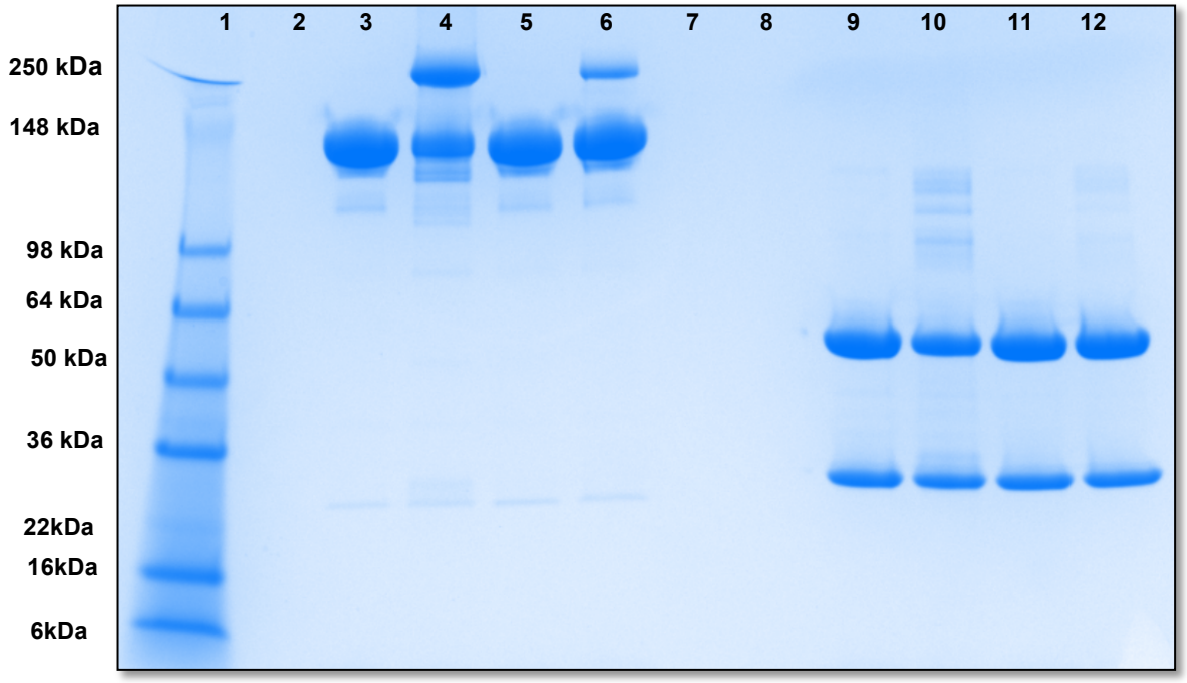

Figure 9—SDS-PAGE of mAb1 monomer and dimer fractions under non-reducing and reducing conditions. SeeBlue Standard Plus2 molecular weight ladder is shown in lane 1. Non-reduced mAb1 thermal monomer, thermal dimer, native monomer and native dimer are shown in lanes 3, 4, 5 and 6, respectively. Reduced mAb1 thermal monomer, thermal dimer, native monomer and native dimer are shown in lanes 9, 10, 11 and 12, respectively. Lanes 2, 7 and 8 are blank controls.

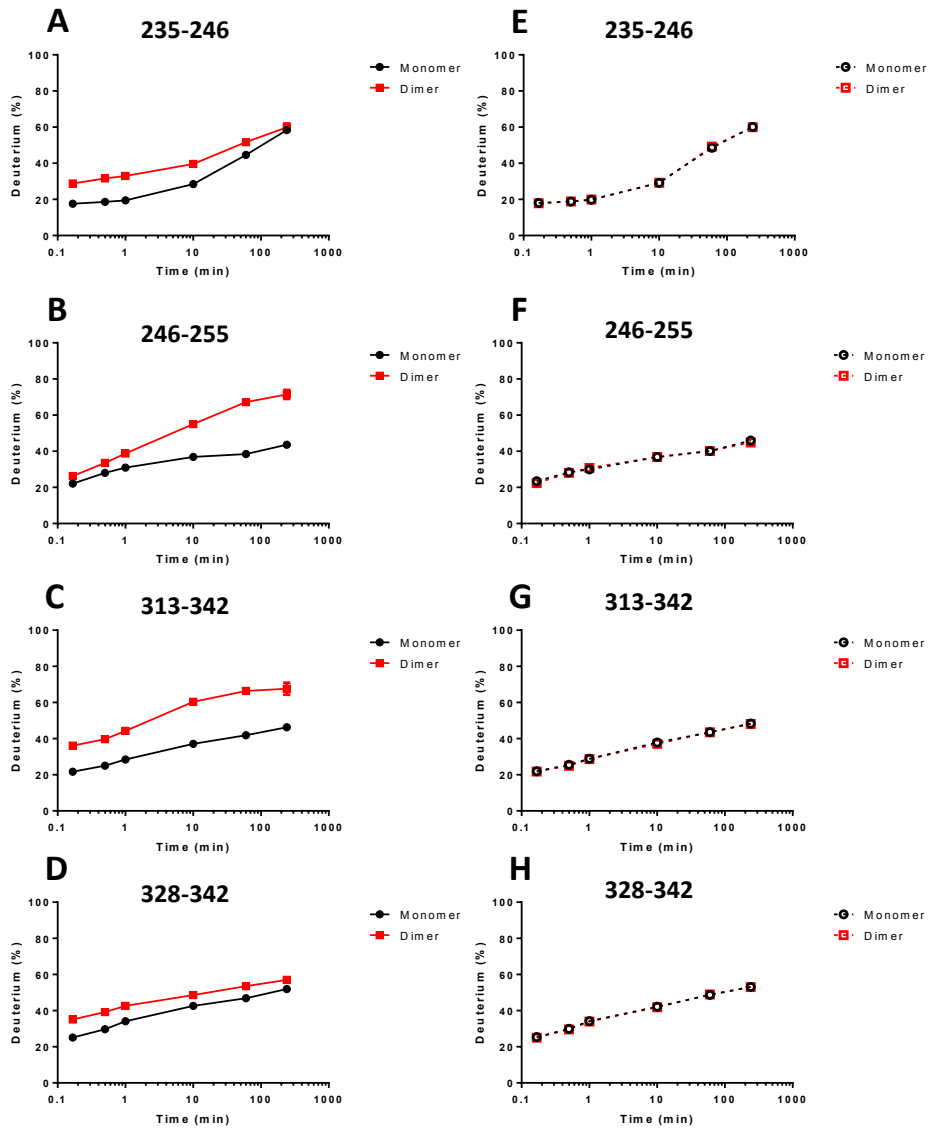

Figure 10—Differences in peptide conformation detected by Hydrogen/Deuterium Exchange Mass Spectrometry (H/D-MS) results. Panels A-D represent peptic peptides for the thermal dimer (red) compared to the native monomer (black). Panels E-H represent same peptic peptides as shown in panels A-D, but for the native dimer (red) compared to the native monomer (black). Amino acid sequence residue numbers are shown for each peptide. The peptides shown in B and D, (with sequences covering residues 246-255 and 313-342, respectively) showed the largest differences in deuterium incorporation and both contain a single cysteine residue responsible for the formation of an intramolecular disulfide bond in the C_H2 domain. The four peptic peptides shown in Panels A-D represent the only peptic peptides with differences in deuterium incorporation rates for all peptides recovered from mAb1 thermal dimer samples compared to mAb1 native monomer.

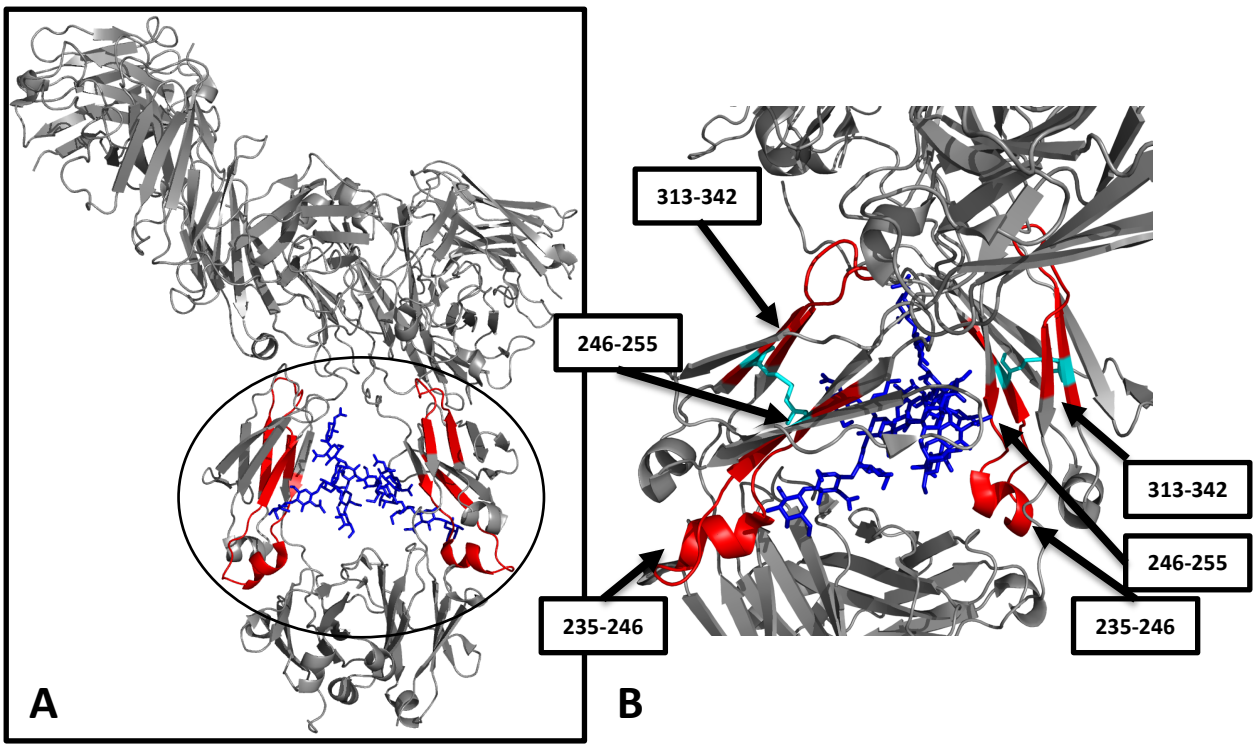

Figure 11—**A three-dimensional (3D) homology model representative of (A) the entire mAb1 structure and (B) the C_H2 domain (see methods section)**. Peptides showing differences in the rate of deuterium uptake in the thermal dimer sample compared to the native monomer are highlighted (red) in the model and identified by their sequence position numbers. The cysteine residues that form the C_H2 intramolecular disulfide bond (cyan) and glycans (blue) are also shown.

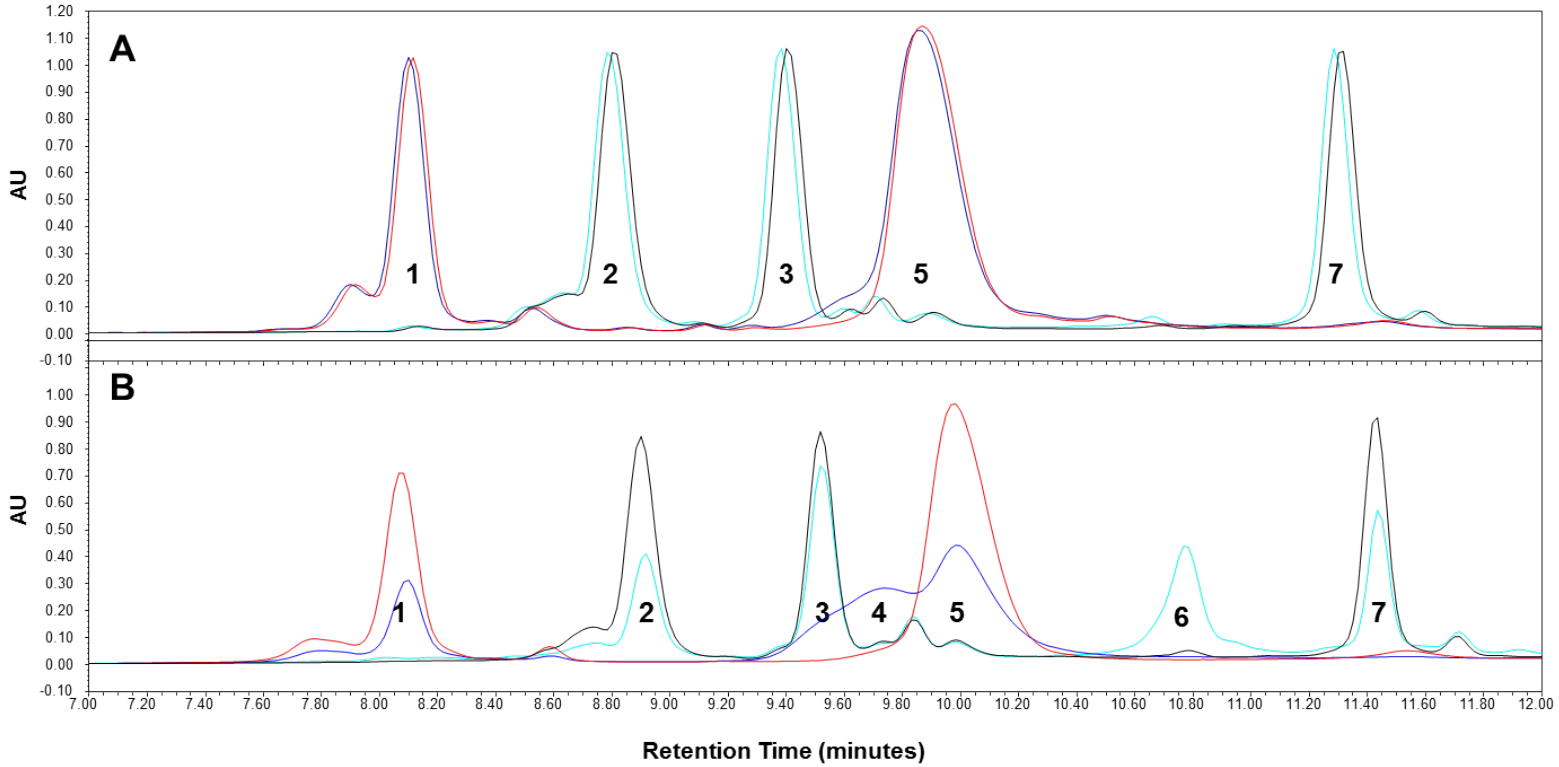

Figure 12. Reversed phase chromatograms for FabRICATOR digests of (A) mAb1 native monomer and native dimer and (B) mAb1 thermal monomer and thermal dimer. Panel A shows mAb1 native monomer FabRICATOR fragments under reducing (black trace) and non-reducing (red trace) conditions. mAb1 native dimer FabRICATOR fragments under reducing (blue trace) and non-reducing (cyan trace) conditions are also shown in panel A. Thermal monomer (red and black traces for non-reducing and reducing conditions, respectively) and thermal dimer (blue and cyan traces for non-reducing and reducing conditions, respectively) mAb1 FabRICATOR fragments are shown in panel B. Peaks identified by mass analysis correspond to the Fc/2 (peak 1, 25232.5 Da, non-reduced), Fc/2 (peak 2, 25237 Da, reduced), LC (peak 3, 23585.7 Da), Fab'2 (peak 5, 95936 Da), and Fd (peak 7, 24392 Da). An unknown peak (4) with a mass too large for mass measurement by the mass spectrometer instrument disappears upon reduction, resulting in the detection of a new peak coinciding with the mass of a single HC (peak 6, 49770 Da).

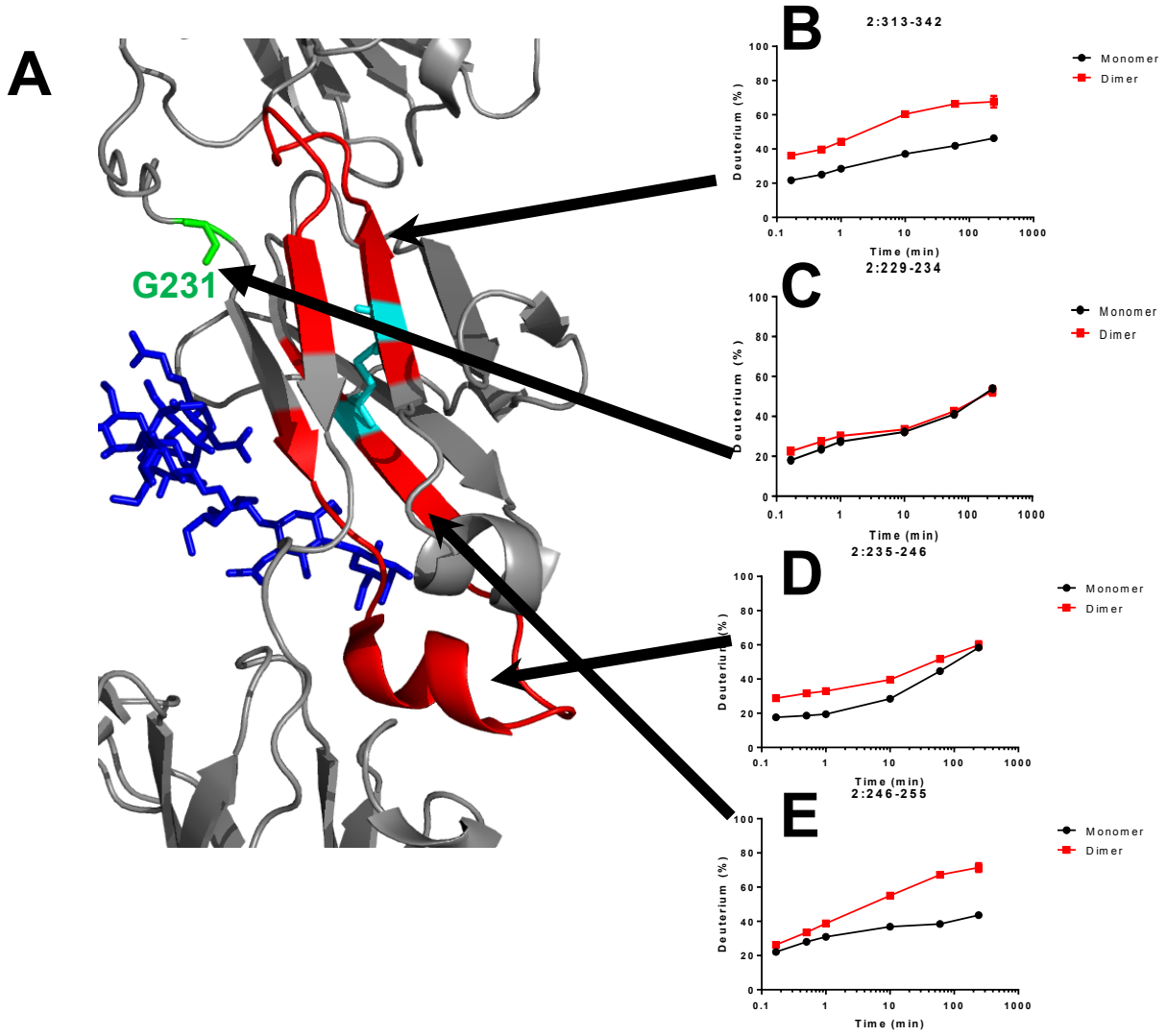

Figure 13—3D model of mAb1 highlighting the C_H2 domain peptides with increased conformational flexibility are located close in proximity to the FabRICATOR enzyme cleavage site. FabRICATOR enzymatic cleavage site (green) is located upstream from the region showing increased flexibility from the H/D-MS results (red). The intramolecular disulfide bond (cyan) and glycans (blue) are highlighted in the 3D homology model shown in panel A. Deuterium uptake rate curves comparing the thermal dimer (red) to native monomer (black) are shown for the peptic peptides corresponding to portions of the mAb1 sequence containing (B) residues 313-342, (C) residues 229-234, (D) residues 235-246 and (E) residues 246-255.

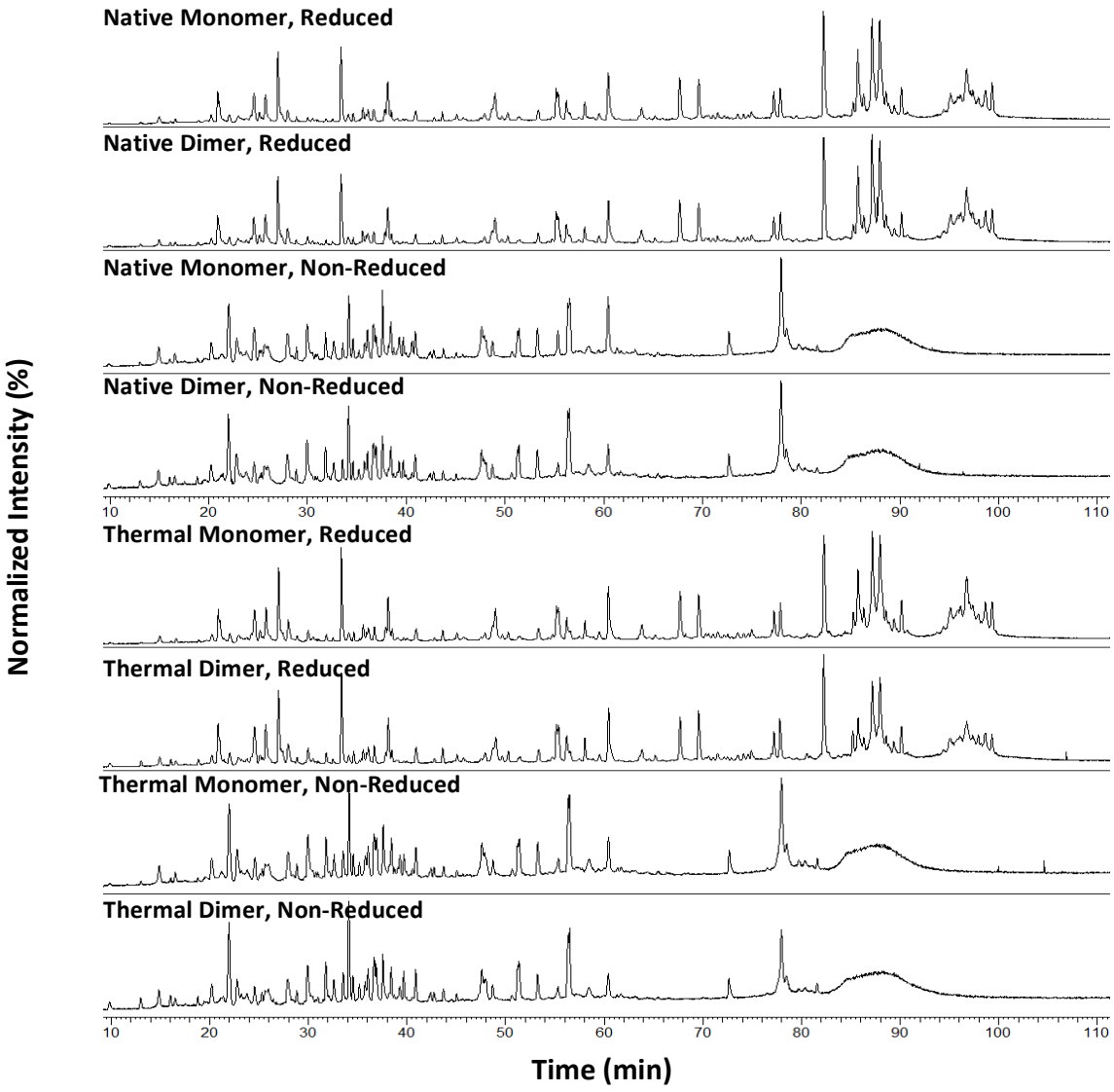

Figure 14—Disulfide bond peptide mapping mass spectra. Reduced and non-reduced peptide maps resulting from Lys-C digests of mAb1 native and thermal monomer and native and thermal dimer fractions. Plots represent normalized intensity as a function of time. Overall, reduced and non-reduced peptide maps of mAb1 monomer and dimer fractions were comparable for both the native species and thermal species. Small differences in intensity are observed, likely attributable to method variability.

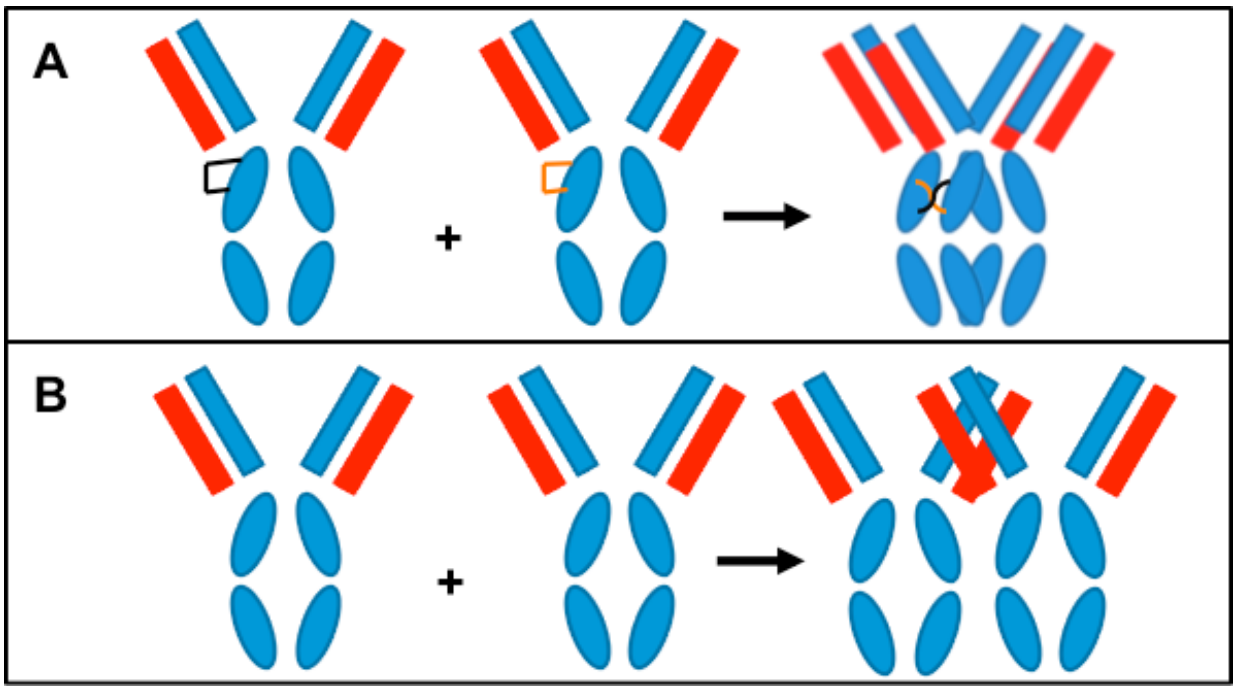

Figure 15—Illustrations explaining potential dimerization mechanisms of mAb1: (a) Domain swapping via the intramolecular disulfide bond of the C_H2 domain and (b) via surface interactions between Fab domains. Intramolecular C_H2 disulfide bonds are highlighted on each mAb monomer and in the intermolecular disulfide bonds in the mAb dimer. It is proposed that during thermal incubation of mAb1 solution, the intramolecular disulfide bond of the C_H2 domain disassociates in several mAb1 monomers within the same timescale. As a consequence, the unpaired cysteine residues on one mAb1 monomer forms the same disulfide bond, but intermolecularly, its respective cysteine residue on a different, adjacent mAb1 monomer in solution. If the disulfide bond domain swapping mechanism leads to the orientation shown in Panel A, then other results of this study, such as the observed spatial orientation by AFM, loss in potency and FcRn binding ability, can be explained. Surface interactions, possibly covalent or non-covalent, between the Fab domain are proposed as being responsible for the observed behavior of mAb1 native dimer species. Since mAb1 native dimer showed reduced potency, it is likely that the Fab domain is structurally altered in such a way as to prevent binding. H/D-MS results indicated that no significant alterations to the protein structure were detected in the Fab region for mAb1 native dimer. Therefore, it is likely that the interactions leading to dimer formation under these conditions involve solvent exposed surface interactions. It was observed that mAb1 native dimer not only retained Fc binding ability, but also showed an increase in binding relative to the mAb1 monomer control. Thus, the model showing two adjacent, but not overlapping Fc portions is consistent with the avidity observed in the FcRn assay. Additionally, such an orientation is consistent with the ~50% reduction in potency and spatial orientation results by AFM.

REFERENCES

1. Walsh, G., *Biopharmaceutical benchmarks 2014.* Nat Biotech, 2014. **32**(10): p. 992-1000.
2. Nose, M. and H. Wigzell, *Biological Significance of Carbohydrate Chains on Monoclonal Antibodies.* Proceedings of the National Academy of Sciences of the United States of America, 1983. **80**(21): p. 6632-6636.
3. Carpenter, J.F., et al., *Overlooking subvisible particles in therapeutic protein products: gaps that may compromise product quality.* J Pharm Sci, 2009. **98**(4): p. 1201-5.
4. Chi, E.Y., et al., *Roles of conformational stability and colloidal stability in the aggregation of recombinant human granulocyte colony-stimulating factor.* Protein Sci, 2003. **12**(5): p. 903-13.
5. Mahler, H.C., et al., *Protein aggregation: pathways, induction factors and analysis.* J Pharm Sci, 2009. **98**(9): p. 2909-34.
6. Mahler, H.C., et al., *Induction and analysis of aggregates in a liquid IgG1-antibody formulation.* Eur J Pharm Biopharm, 2005. **59**(3): p. 407-17.
7. Shire, S.J., *Formulation and manufacturability of biologics.* Curr Opin Biotechnol, 2009. **20**(6): p. 708-14.
8. Cleland, J.L., M.F. Powell, and S.J. Shire, *The development of stable protein formulations: a close look at protein aggregation, deamidation, and oxidation.* Crit Rev Ther Drug Carrier Syst, 1993. **10**(4): p. 307-77.
9. Fradkin, A.H., J.F. Carpenter, and T.W. Randolph, *Immunogenicity of aggregates of recombinant human growth hormone in mouse models.* J Pharm Sci, 2009. **98**(9): p. 3247-64.
10. Patapoff, T.W. and O. Esue, *Polysorbate 20 prevents the precipitation of a monoclonal antibody during shear.* Pharm Dev Technol, 2009. **14**(6): p. 659-64.
11. Tyagi, A.K., et al., *IgG particle formation during filling pump operation: a case study of heterogeneous nucleation on stainless steel nanoparticles.* J Pharm Sci, 2009. **98**(1): p. 94-104.
12. Andya, J.D., C.C. Hsu, and S.J. Shire, *Mechanisms of aggregate formation and carbohydrate excipient stabilization of lyophilized humanized monoclonal antibody formulations.* AAPS PharmSci, 2003. **5**(2): p. E10.
13. Bee, J.S., et al., *Response of a concentrated monoclonal antibody formulation to high shear.* Biotechnol Bioeng, 2009. **103**(5): p. 936-43.
14. Benjwal, S., et al., *Monitoring protein aggregation during thermal unfolding in circular dichroism experiments.* Protein Sci, 2006. **15**(3): p. 635-9.
15. Bond, M.D., et al., *Evaluation of a dual‐wavelength size exclusion HPLC method with improved sensitivity to detect protein aggregates and its use to better characterize degradation pathways of an IgG1 monoclonal antibody.* Journal of Pharmaceutical Sciences, 2010. **99**(6): p. 2582-2597.
16. Brych, S.R., et al., *Characterization of antibody aggregation: Role of buried, unpaired cysteines in particle formation.* Journal of Pharmaceutical Sciences, 2010. **99**(2): p. 764-781.

17. Roberts, C.J., T.K. Das, and E. Sahin, *Predicting solution aggregation rates for therapeutic proteins: Approaches and challenges.* International Journal of Pharmaceutics, 2011. **418**(2): p. 318-333.
18. Narhi, L.O., et al., *Classification of protein aggregates.* Journal of Pharmaceutical Sciences, 2012. **101**(2): p. 493-498.
19. Johansen, F.E., R. Braathen, and P. Brandtzaeg, *Role of J chain in secretory immunoglobulin formation.* Scand J Immunol, 2000. **52**(3): p. 240-8.
20. Ramani, K., et al., *Aggregation kinetics of recombinant human FVIII (rFVIII).* J Pharm Sci, 2005. **94**(9): p. 2023-9.
21. Remmele, R.L., Jr., et al., *Active dimer of Epratuzumab provides insight into the complex nature of an antibody aggregate.* J Pharm Sci, 2006. **95**(1): p. 126-45.
22. Wang, W., *Instability, stabilization, and formulation of liquid protein pharmaceuticals.* Int J Pharm, 1999. **185**(2): p. 129-88.
23. Van Buren, N., et al., *Elucidation of two major aggregation pathways in an IgG2 antibody.* J Pharm Sci, 2008.
24. Deperalta, G., et al. *Structural analysis of a therapeutic monoclonal antibody dimer by hydroxyl radical footprinting*. in *MAbs*. 2013. Taylor & Francis.
25. Moore, J.M., T.W. Patapoff, and M.E. Cromwell, *Kinetics and thermodynamics of dimer formation and dissociation for a recombinant humanized monoclonal antibody to vascular endothelial growth factor.* Biochemistry, 1999. **38**(42): p. 13960-13967.
26. Lau, H., et al., *Investigation of degradation processes in IgG1 monoclonal antibodies by limited proteolysis coupled with weak cation-exchange HPLC.* Journal of Chromatography B, 2010. **878**(11): p. 868-876.
27. Kanai, S., et al., *Reversible self-association of a concentrated monoclonal antibody solution mediated by Fab-Fab interaction that impacts solution viscosity.* J Pharm Sci, 2008. **97**(10): p. 4219-27.
28. Zheng, K., C.R. Middaugh, and T.J. Siahaan, *Evaluation of the physical stability of the EC5 domain of E-cadherin: effects of pH, temperature, ionic strength, and disulfide bonds.* J Pharm Sci, 2009. **98**(1): p. 63-73.
29. Paul, R., et al., *Structure and function of purified monoclonal antibody dimers induced by different stress conditions.* Pharm Res, 2012. **29**(8): p. 2047-59.
30. Iacob, R.E., et al., *Investigating Monoclonal Antibody Aggregation Using a Combination of H/DX–MS and Other Biophysical Measurements.* Journal of Pharmaceutical Sciences, 2013. **102**(12): p. 4315-4329.
31. Zhang, A., et al., *Understanding the conformational impact of chemical modifications on monoclonal antibodies with diverse sequence variation using hydrogen/deuterium exchange mass spectrometry and structural modeling.* Analytical chemistry, 2014. **86**(7): p. 3468-3475.
32. den Engelsman, J., et al., *Strategies for the Assessment of Protein Aggregates in Pharmaceutical Biotech Product Development.* Pharm Res, 2011. **28**(4): p. 920-933.
33. Berkowitz, S., *Role of analytical ultracentrifugation in assessing the aggregation of protein biopharmaceuticals.* The AAPS Journal, 2006. **8**(3): p. E590-E605.
34. Stine, W.B., Jr., *Analysis of Monoclonal Antibodies by Sedimentation Velocity Analytical Ultracentrifugation*, in *Glycosylation Engineering of Biopharmaceuticals*, A. Beck, Editor. 2013, Humana Press. p. 227-240.

35. Wang, T., et al., *Case studies applying biophysical techniques to better characterize protein aggregates and particulates of varying size*, in *Biophysics for Therapeutic Protein Development*. 2013, Springer. p. 205-243.
36. Filipe, V., et al., *Transient molten globules and metastable aggregates induced by brief exposure of a monoclonal IgG to low pH.* J Pharm Sci, 2012. **101**(7): p. 2327-39.
37. Greenfield, N.J., *Using circular dichroism spectra to estimate protein secondary structure.* Nature protocols, 2006. **1**(6): p. 2876-2890.
38. Ricci, M.S., et al., *pH Dependence of structural stability of interleukin-2 and granulocyte colony-stimulating factor.* Protein Sci, 2003. **12**(5): p. 1030-8.
39. Vermeer, A.W. and W. Norde, *The thermal stability of immunoglobulin: unfolding and aggregation of a multi-domain protein.* Biophys J, 2000. **78**(1): p. 394-404.
40. Vermeer, A.W., W. Norde, and A. van Amerongen, *The unfolding/denaturation of immunogammaglobulin of isotype 2b and its F(ab) and F(c) fragments.* Biophys J, 2000. **79**(4): p. 2150-4.
41. Whitmore, L. and B.A. Wallace, *Protein secondary structure analyses from circular dichroism spectroscopy: Methods and reference databases.* Biopolymers, 2008. **89**(5): p. 392-400.
42. Li, C.H., et al., *Applications of circular dichroism (CD) for structural analysis of proteins: qualification of near- and far-UV CD for protein higher order structural analysis.* Journal of Pharmaceutical Sciences, 2011. **100**(11): p. 4642-4654.
43. Barth, A., *Infrared spectroscopy of proteins.* Biochimica et Biophysica Acta (BBA) - Bioenergetics, 2007. **1767**(9): p. 1073-1101.
44. Chang, L.L., et al., *Mechanism of protein stabilization by sugars during freeze-drying and storage: native structure preservation, specific interaction, and/or immobilization in a glassy matrix?* J Pharm Sci, 2005. **94**(7): p. 1427-44.
45. Harn, N., et al., *Highly concentrated monoclonal antibody solutions: direct analysis of physical structure and thermal stability.* J Pharm Sci, 2007. **96**(3): p. 532-46.
46. Jiang, Y., et al., *Qualification of FTIR spectroscopic method for protein secondary structural analysis.* Journal of pharmaceutical sciences, 2011. **100**(11): p. 4631-4641.
47. Telikepalli, S.N., et al., *Structural characterization of IgG1 mAb aggregates and particles generated under various stress conditions.* Journal of Pharmaceutical Sciences, 2014. **103**(3): p. 796-809.
48. Tian, F., et al., *Spectroscopic evaluation of the stabilization of humanized monoclonal antibodies in amino acid formulations.* Int J Pharm, 2007. **335**(1-2): p. 20-31.
49. He, F., et al., *High-Throughput Biophysical Approaches to Therapeutic Protein Development*, in *Biophysics for Therapeutic Protein Development*, L.O. Narhi, Editor. 2013, Springer New York. p. 7-31.
50. Hawe, A., M. Sutter, and W. Jiskoot, *Extrinsic Fluorescent Dyes as Tools for Protein Characterization.* Pharm Res, 2008. **25**(7): p. 1487-1499.
51. He, F., et al., *High throughput thermostability screening of monoclonal antibody formulations.* J Pharm Sci, 2010. **99**(4): p. 1707-20.
52. He, F., et al., *Detection of IgG aggregation by a high throughput method based on extrinsic fluorescence.* Journal of pharmaceutical sciences, 2010. **99**(6): p. 2598-2608.
53. Gill, P., T.T. Moghadam, and B. Ranjbar, *Differential Scanning Calorimetry Techniques: Applications in Biology and Nanoscience.* Journal of Biomolecular Techniques : JBT, 2010. **21**(4): p. 167-193.

54. Ionescu, R.M., et al., *Contribution of variable domains to the stability of humanized IgG1 monoclonal antibodies.* J Pharm Sci, 2008. **97**(4): p. 1414-26.
55. Buchanan, A., et al., *Engineering a therapeutic IgG molecule to address cysteinylation, aggregation and enhance thermal stability and expression.* mAbs, 2013. **5**(2): p. 255-262.
56. Chennamsetty, N., et al., *Design of therapeutic proteins with enhanced stability.* Proceedings of the National Academy of Sciences, 2009. **106**(29): p. 11937-11942.
57. Banks, D.D., et al., *Native-state solubility and transfer free energy as predictive tools for selecting excipients to include in protein formulation development studies.* Journal of Pharmaceutical Sciences, 2012. **101**(8): p. 2720-2732.
58. Hari, S.B., et al., *Acid-Induced Aggregation of Human Monoclonal IgG1 and IgG2: Molecular Mechanism and the Effect of Solution Composition.* Biochemistry, 2010. **49**(43): p. 9328-9338.
59. Majumdar, R., et al., *Hydrogen–Deuterium Exchange Mass Spectrometry as an Emerging Analytical Tool for Stabilization and Formulation Development of Therapeutic Monoclonal Antibodies.* Journal of Pharmaceutical Sciences, 2015. **104**(2): p. 327-345.
60. Zhang, Z., A. Zhang, and G. Xiao, *Improved Protein Hydrogen/Deuterium Exchange Mass Spectrometry Platform with Fully Automated Data Processing.* Analytical Chemistry, 2012. **84**(11): p. 4942-4949.
61. Magliery, T.J., J.J. Lavinder, and B.J. Sullivan, *Protein stability by number: high-throughput and statistical approaches to one of protein science's most difficult problems.* Current Opinion in Chemical Biology, 2011. **15**(3): p. 443-451.
62. Zhang, J., et al., *Hydrogen/deuterium exchange reveals distinct agonist/partial agonist receptor dynamics within vitamin D receptor/retinoid X receptor heterodimer.* Structure, 2010. **18**(10): p. 1332-1341.
63. Chalmers, M.J., et al., *Probing protein ligand interactions by automated hydrogen/deuterium exchange mass spectrometry.* Analytical chemistry, 2006. **78**(4): p. 1005-1014.
64. Banks, D.D., J. Zhang, and C.C. Siska, *Relationship between native-state solubility and non-native aggregation of recombinant human granulocyte colony stimulating factor: Practical implications for protein therapeutic development.* Molecular pharmaceutics, 2014. **11**(10): p. 3431-3442.
65. Manikwar, P., et al., *Correlating excipient effects on conformational and storage stability of an IgG1 monoclonal antibody with local dynamics as measured by hydrogen/deuterium-exchange mass spectrometry.* Journal of Pharmaceutical Sciences, 2013. **102**(7): p. 2136-2151.
66. Arora, J., et al. *Hydrogen exchange mass spectrometry reveals protein interfaces and distant dynamic coupling effects during the reversible self-association of an IgG1 monoclonal antibody*. in *mAbs*. 2015. Taylor & Francis.
67. Tang, L., et al. *Conformational characterization of the charge variants of a human IgG1 monoclonal antibody using H/D exchange mass spectrometry*. in *MAbs*. 2013. Taylor & Francis.
68. Majumdar, R., et al., *Hydrogen-deuterium exchange mass spectrometry as an emerging analytical tool for stabilization and formulation development of therapeutic monoclonal antibodies.* J Pharm Sci, 2015. **104**(2): p. 327-45.

69. Schuck, P., et al., *Size-Distribution Analysis of Proteins by Analytical Ultracentrifugation: Strategies and Application to Model Systems.* Biophysical Journal, 2002. **82**(2): p. 1096-1111.
70. Gabrielson, J.P., et al., *Precision of protein aggregation measurements by sedimentation velocity analytical ultracentrifugation in biopharmaceutical applications.* Analytical Biochemistry, 2010. **396**(2): p. 231-241.
71. He, F., et al., *Detection of IgG aggregation by a high throughput method based on extrinsic fluorescence.* J Pharm Sci, 2010. **99**(6): p. 2598-608.
72. Saphire, E.O., et al., *Crystal structure of a neutralizing human IGG against HIV-1: a template for vaccine design.* Science, 2001. **293**(5532): p. 1155-9.
73. Datta-Mannan, A., et al., *FcRn Affinity-Pharmacokinetic Relationship of Five Human IgG4 Antibodies Engineered for Improved In Vitro FcRn Binding Properties in Cynomolgus Monkeys.* Drug Metabolism and Disposition, 2012. **40**(8): p. 1545-1555.
74. Nagashima, H., et al., *Tandemly repeated Fc domain augments binding avidities of antibodies for Fcγ receptors, resulting in enhanced antibody-dependent cellular cytotoxicity.* Molecular immunology, 2008. **45**(10): p. 2752-2763.
75. Schlothauer, T., et al., *Analytical FcRn affinity chromatography for functional characterization of monoclonal antibodies.* mAbs, 2013. **5**(4): p. 576-586.
76. Dower, S.K., et al., *Mechanism of binding of multivalent immune complexes to Fc receptors. 1. Equilibrium binding.* Biochemistry, 1981. **20**(22): p. 6326-6334.
77. Goldberg, D.S., et al., *Formulation development of therapeutic monoclonal antibodies using high-throughput fluorescence and static light scattering techniques: Role of conformational and colloidal stability.* Journal of pharmaceutical sciences, 2011. **100**(4): p. 1306-1315.
78. Senisterra, G.A. and P.J. Finerty Jr, *High throughput methods of assessing protein stability and aggregation.* Molecular Biosystems, 2009. **5**(3): p. 217-223.
79. Chevreux, G., N. Tilly, and N. Bihoreau, *Fast analysis of recombinant monoclonal antibodies using IdeS proteolytic digestion and electrospray mass spectrometry.* Analytical Biochemistry, 2011. **415**(2): p. 212-214.
80. Jaskolski, M., *3D domain swapping–implications for conformational disorders and ways of control.* BioTechnologia. Journal of Biotechnology Computational Biology and Bionanotechnology, 2011. **92**(1).
81. West, A.P., Jr., et al., *Design and expression of a dimeric form of human immunodeficiency virus type 1 antibody 2G12 with increased neutralization potency.* J Virol, 2009. **83**(1): p. 98-104.
82. Bennett, M.J., S. Choe, and D. Eisenberg, *Domain swapping: entangling alliances between proteins.* Proc Natl Acad Sci U S A, 1994. **91**(8): p. 3127-31.
83. Orlikowska, M., et al., *Hinge-loop mutation can be used to control 3D domain swapping and amyloidogenesis of human cystatin C.* J Struct Biol, 2011. **173**(2): p. 406-13.
84. Rousseau, F., J. Schymkowitz, and L.S. Itzhaki, *Implications of 3D domain swapping for protein folding, misfolding and function.* Adv Exp Med Biol, 2012. **747**: p. 137-52.
85. Arnold, J.N., et al., *The impact of glycosylation on the biological function and structure of human immunoglobulins.* Annu. Rev. Immunol., 2007. **25**: p. 21-50.
86. Monnet, C., et al., *Selection of IgG Variants with Increased FcRn Binding Using Random and Directed Mutagenesis: Impact on Effector Functions.* Frontiers in Immunology, 2015. **6**: p. 39.

87. Monnet, C., et al., *Combined glyco- and protein-Fc engineering simultaneously enhance cytotoxicity and half-life of a therapeutic antibody.* MAbs, 2014. **6**(2): p. 422-36.
88. Wypych, J., et al., *Human IgG2 Antibodies Display Disulfide-mediated Structural Isoforms.* Journal of Biological Chemistry, 2008. **283**(23): p. 16194-16205.
89. Zhang, A., et al., *Conformational Difference in Human IgG2 Disulfide Isoforms Revealed by Hydrogen/Deuterium Exchange Mass Spectrometry.* Biochemistry, 2015. **54**(10): p. 1956-1962.
90. Liu, H., et al., *Characterization of lower molecular weight artifact bands of recombinant monoclonal IgG1 antibodies on non-reducing SDS-PAGE.* Biotechnology Letters, 2007. **29**(11): p. 1611-1622.
91. Zhang, A., et al., *Distinct Aggregation Mechanisms of Monoclonal Antibody Under Thermal and Freeze-Thaw Stresses Revealed by Hydrogen Exchange.* Pharmaceutical Research, 2012. **29**(1): p. 236-250.